The double structure of the Estuarine Turbidity Maximum in the Cam-Nam Trieu mesotidal tropical estuary, Vietnam

Vu Duy Vinh, Sylvain Ouillon

Marine Geology 442 (2021) 106670

Contents lists available at ScienceDirect

Marine Geology

journal homepage: www.elsevier.com/locate/margo

The double structure of the Estuarine Turbidity Maximum in the Cam-Nam Trieu mesotidal tropical estuary, Vietnam

Vu Duy Vinh [a,*], Sylvain Ouillon [b,c,**]

[a] Institute of Marine Environment and Resources, Vietnamese Academy of Science and Technology (VAST), 246 Danang Street, Haiphong City, Viet Nam
[b] UMR LEGOS, Université de Toulouse, IRD, CNES, CNRS, UPS, 14 avenue Edouard Belin, 31400 Toulouse, France
[c] Department Water-Environment-Oceanography, University of Science and Technology of Hanoi (USTH), Vietnamese Academy of Science and Technology (VAST), 18 Hoang Quoc Viet, Hanoi 100000, Viet Nam

ARTICLE INFO

Editor: Prof Edward Anthony

Keywords:
Estuarine turbidity maximum
Estuaries
Suspended sediment
Settling velocity
Excess of density
Fractal dimension

ABSTRACT

The characteristic parameters of the Estuarine Turbidity Maxima (ETM), their aggregates and their tidal variations were investigated within the Cam-Nam Trieu mesotidal estuary (Red River and Thai Binh River system, North Vietnam) at spring tides during the early wet season, wet season and dry season. The structure observed repeatedly highlights the separation of two distinct zones of high turbidity around the salt wedge, separated by a zone of lower turbidity. The upstream part developed at very low salinity (from 0.1 psu) on a quasi-homogeneous water column (at Simpson parameter between ~0.65 and 7–10); tidal pumping associated with salinity-induced flocculation are likely responsible for its formation. A second maximum was observed in the lower layer of stratified waters (at Simpson parameters >10), i.e. in the salt wedge, at higher salinities up to ~12–15 psu; in this downstream part, governed by the gravitational circulation, settling is also seasonally enhanced by the presence of transparent exopolymeric particles (TEP) for salinity >10 psu. Turbidity was higher in the upper part of ETM in the dry season and higher in the lower part of ETM in the wet season. Floc size, excess of density and settling velocity were the highest during dry season. Stronger ETMs occur in dry season than in early wet season and wet season, when the tidal-induced ETM is maximum. The locations of both ETM parts changed seasonally, moving upstream in the dry season and downstream in the wet season. Their length depended on the longitudinal salinity gradient and was highest at low tide than at high tide. The intermediate zone of lower turbidity between these two parts was longer in the wet season.

1. Introduction

Estuarine Turbidity Maxima (ETMs) are zones of elevated suspended particulate matter (SPM) concentration at the interface between the river and the sea. Because of the strong influences of marine water, tide and river discharge, the occurrence of ETMs is complex (Fettweis et al., 1998; Mitchell and Uncles, 2013). They are trapping a lot of suspended matter and encompass a huge range of SPM concentrations with maximum values from less than 100 mg L^{-1} like in the Kennebec Estuary, USA (Kistner and Pettigrew, 2001; Uncles et al., 2002) to >200 g L^{-1} like in the Severn Estuary, UK (Kirby and Parker, 1983). The settling of SPM in an ETM has been well documented in the Gironde estuary (Allen and Castaing, 1973; Sottolichio and Castaing, 1999; Jalón-Rojas et al., 2015), the Hudson estuary (Olsen et al., 1978; Geyer et al., 2001; Traykovski et al., 2004), the Columbia River estuary (Jay and Musiak, 1994), the Seine estuary (Brenon and Le Hir, 1999), the Chesapeake Bay (Sanford et al., 2001; Sanford et al., 2005), and the Humber estuary (Uncles et al., 2006), amongst others. For instance, Olsen et al. (1978) showed that the deposition rate reached up to 30 cm $year^{-1}$ in certain parts of the ETM in the Hudson estuary on timescales of 5–10 years.

Most of the time, the turbidity maximum area is located at the boundary between river water and sea water (Allen and Castaing, 1973; Uncles and Stephens, 1993; Geyer et al., 2001; Sanford et al., 2005). When there is little tidal motion, the longitudinal pressure gradient or surface slope (barotropic force) compensates the longitudinal density gradient (baroclinic force). Since the barotropic force is vertically homogeneous and acts in down-estuary direction, while the baroclinic force increases with depth and acts in an up-estuary direction, their

* Corresponding author.
** Corresponding author at: UMR LEGOS, Université de Toulouse, IRD, CNES, CNRS, UPS, 14 avenue Edouard Belin, 31400 Toulouse, France.
E-mail addresses: vinhvd@imer.vast.vn (V.D. Vinh), sylvain.ouillon@legos.obs-mip.fr (S. Ouillon).

https://doi.org/10.1016/j.margeo.2021.106670
Received 25 December 2020; Received in revised form 1 October 2021; Accepted 7 October 2021
Available online 11 October 2021

combination creates the "estuarine circulation" (Officer, 1981; Dyer, 1995). The convergence at the saltfront of seaward sediment flux by the river flow and landward sediment flux by the gravitational circulation is considered as a fundamental mechanism contributing to ETM formation (Postma, 1967; Bowden, 1984; Toublanc et al., 2016), even in the absence of tidal effects, as shown by Festa and Hansen (1978). However, in most estuaries, resuspension induced by tidal asymmetry has also been recognized as a key factor in maintaining high SPM concentration (Schubel, 1968; Allen et al., 1980; Brenon and Le Hir, 1999; Sottolichio et al., 2000). Flood tide, which is generally shorter and more energetic than the ebb tide in estuaries, is able to put sediment into suspension and bring them back landward. Vertical mixing is also enhanced during the flood and lowered in the more stratified ebb waters (Coleman and Wright, 1978). As a consequence, sediment transport is greater during the flood than during the ebb tide (Allen et al., 1980; Mitchell, 2013).

Due to change of conditions such as river discharge, SPM concentration, water temperature and salinity, the characteristics of ETMs (pattern, maximum turbidity, location, length) and aggregate parameters vary seasonally. From measurements in a coastal turbidity maximum area (southern North Sea), Fettweis and Baeye (2015) reported that the seasonality was mainly caused by changes in floc size and settling velocity, with smaller flocs and thus settling velocities in winter and larger flocs and settling velocities in summer. In the Dollard estuary in the Netherlands, van der Lee (2000) showed that SPM concentration and turbulence mainly affected the tidal variation of floc size, and that biological processes impacted the seasonal floc size variation but very few the floc settling velocities, since an increase in floc size was mainly counterbalanced by a decrease in floc density. Verney et al. (2009) showed that the constituents of the suspended sediments and their content in organic matter have a major effect on seasonality of flocculation processes (efficiency, speed and time) in the Seine estuary. From 3 years of measurements in the Humber-Ouse estuary, Uncles et al. (1999) reported that the ETM moved more than 60 km up estuary during the drought of summer 1995 as compared to the previous winter. They also showed that the Humber-Ouse ETM was weaker and further down-estuary in winter than during summer and early autumn, when it was stronger and much closer to the tidal limit. Other studies show seasonal variations of ETM characteristics, most of them in temperate areas.

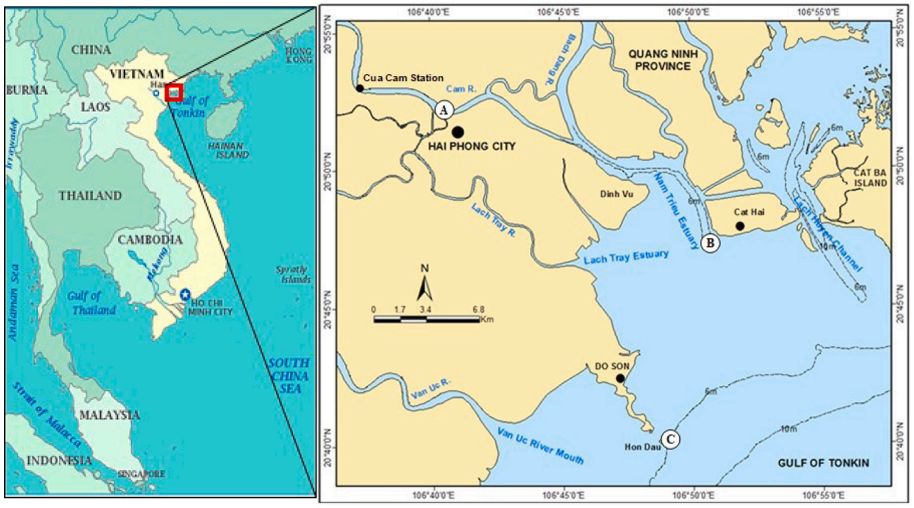

(a)

(b)

Fig. 1. The Cam-Nam Trieu estuary (a) general location – transects were performed between stations A and B, Cua Cam Station is the hydrological station, C is the tide gauge at Hon Dau; (b) example of survey (stations of Transect 3 in Sep 2015) along the A-B transect.

Tropical estuaries (between 30°N and 30°S of latitude) are fringed by mangrove forests and their dynamics can be largely affected by coastal migration of mud banks as along the French Guiana coast (e.g., Orseau et al., 2017). The variability and strength of their forcing may also be different, due to the strong seasonal variation associated with the monsoon and the occurrence of extreme events (typhoons). Few studies have been published on the dynamics of ETM in tropical estuaries: Wolanski et al. (1996) outlined the seasonal variations of the turbidity maximum in the Mekong estuary; Capo et al. (2006) showed that the ETM of the Konkouré estuary was river-controlled and correlated with the residual currents but not with the salinity front; Abascal-Zorrilla et al. (2020) analyzed seasonal and lunar (neap-spring tides) variations in the remotely-sensed ETM location of the Maroni river from Landsat-8 data; but very few studies have described at once the variations of ETM patterns and aggregate characteristics.

The Cam-Nam Trieu estuary (Fig. 1a), located in Hai Phong city (Northeast Vietnam) and belonging to the Red River and Thai Binh River basins, is an interesting site to study estuarine dynamics under tropical climate because this mesotidal estuary is both influenced by a strong seasonal river signal and a monsoon regime (Duy Vinh et al., 2018). Furthermore, its tidal asymmetry is strong, with negative (or upward) flow between 24% of time (in wet season) and 45% (in dry season), and shorter flood than ebb tides (Lefebvre et al., 2012).

Hydro-sedimentary processes in the Red River estuaries have been the subject of previous work. Vinh et al. (2014) analyzed the interannual variability of sediment fluxes in the main river and its distributaries; Lefebvre et al. (2012) highlighted tidal pumping in the estuary and showed the control of turbulence on floc size during a tidal cycle; Mari et al. (2012) showed that bio-aggregation was enhanced at 10–15 psu during the summer; Piton et al. (2020b) detailed the variations in aggregate characteristics at three estuarine stations spaced 10-km apart during a tidal cycle, during spring and neap tides and in the wet and dry seasons. Duy Vinh et al. (2018) started to analyze the spatial variability of physical forcing and aggregate characteristics along transects in the Cam-Nam Trieu estuary during the early wet season at spring tides. They reported that two types of ETM had been sampled and observed: an upper well mixed ETM with high SPM concentrations up to the surface developed at low salinity (0.11 to <1 psu), while a lower ETM was confined in a bottom layer over stratified waters at salinities between ~1 psu and 15 psu – "up" and "low" referring here to two different parts of the estuary. The characteristics of ETM parts and aggregate parameters were shown to significantly vary at the tidal scale. Additional measurements of several parameters of the ETM or driving the formation of the turbidity maximum such as SPM concentration, floc size, settling velocity, salinity and velocity were measured in wet and dry seasons, at spring tides. This paper aims at synthesizing the main results, analyzing the seasonal variations of ETM characteristics and aggregate parameters along the Cam-Nam Trieu estuary at spring tides, and outlining the processes that control them.

2. The Cam-Nam Trieu Estuary

Hai Phong ports system is the second biggest port in Vietnam, the main gate of the North Vietnam to the world. This harbor is located along the Cam-Nam Trieu estuary (Fig. 1a). This estuary receives water and sediment from the Cam River and the Bach Dang River. Their confluence is located around 5 km from the river mouth. The total river discharge through the Nam Trieu estuary to the coastal zone is about 20 $\times$ 10^9 m^3 $year^{-1}$, corresponding to 16.5% of the total water discharge from the Red River system to the Tonkin Gulf (Vinh et al., 2014).

Particle Size Distribution of bed sediments are bimodal and show a mixture of fine sediment (peaking around 8–9 μm) and of sand around 140–220 μm (Lefebvre et al., 2012). Most of the area is covered by sandy silt (55–66% of silt, 16–27% of sand) with D_{50} ~ 10–17 μm, except in a small area between the Cam-Bach Dang confluence and the river mouth composed of muddy sand (D_{50} = 140 μm), and a silty area (74% of silt, 21% of clay and 5% of sand; D_{50} = 7.8 μm) at the middle of the Haiphong Bay, around 8 km offshore the river mouth.

The sediment flux from the Red-Thai Binh River basin through the Cam and Bach Dang Rivers to the coastal zones was about 13.2 $\times$ 10^6 t $year^{-1}$, until the Hoa Binh dam impoundment in the 1980s. Vinh et al. (2014) reported that a large amount of riverine sediment has been trapped in the reservoirs since then: the sediment flux through the Cam and Bach Dang Rivers to the coastal zones decreased to 6.0 $\times$ 10^6 t $year^{-1}$, in proportion to 17% of the total sediment flux from the Red River to the coastal waters.

The Cam-Nam Trieu estuary is under the influence of a tropical monsoon climate with alternation of wet summers and dry winters. Annual rainfall in the region (based on measurements at Hon Dau, 1978–2007, see location in Fig. 1a) is 1161 mm, of which nearly 80% falls during the summer monsoon (May to October) and only 8.3% during the winter monsoon (Dec.-March). The wind direction is dominantly (72.2%) from the East (NE, E, SE) and South (SW, S, SE) directions in summer (June to September), and from the North (NE, N, NW) and East (SE, E, NE) directions (92.1%) in dry season (December to March), from wind data measured at Hon Dau (1960–2011) (Duy Vinh et al., 2018).

The Cam and Bach Dang Rivers are strongly affected by hydrological regime of the Red River. Based on data from 1960 to 2010, the Red River discharge at Son Tay (near the apex of the Red River delta) varied from year to year over the range 80.5 (in 2010)–160.7 (in 1971) $\times$ 10^9 m^3 $year^{-1}$, with an average value of 110.0 $\times$ 10^9 m^3 $year^{-1}$ (Duy Vinh et al., 2018). Seasonal variations in water flow are strong, with in average 70.4% of annual flow in the rainy season (June to October) and 17.1% in the dry season (December to April) (Vinh et al., 2014). The Cam-Nam Trieu estuary is affected by tides which are mainly diurnal (Minh et al., 2014; Piton et al., 2020a). Based on tide gauge measurements at Hon Dau station (1960–2011, position C in Fig. 1a located ~14 km from the river mouth), tidal range is about 2.6–3.6 m in spring tide and about 0.5–1.0 m in neap tide (Vinh et al., 2014).

The Cam-Nam Trieu estuary is strongly influenced by tidal propagation. Several mechanisms are responsible of the tidal asymmetry, such as the higher wave celerity (prop. to $\sqrt{gh}$) at high water level than at low water level, and the difference of bottom friction at high and low water levels. As a result, flood tide is shorter than the ebb tide in the Cam-Nam Trieu estuary (Lefebvre et al., 2012). The tidal asymmetry can also be illustrated from water level and water discharge measurements at the hydrologic Cua Cam station in the estuary (see its location in Fig. 1-a) in dry season (January 2016) at spring tide: the flood period (defined as increasing water elevation) lasted 9 to 10 h, while ebb tide lasted 14 to 15 h at spring tide (Fig. 2).

3. Material and methods

3.1. Field data

Three field surveys were performed in the Cam-Nam Trieu estuary at spring tides during the early wet season (10–13 May 2015), wet season (23–25 September 2015) and dry season (11–12 January 2016). Over these three surveys, 15 transects (6 in early wet season; 5 in wet season and 4 in dry season) were recorded, including 310 stations. Along river transects were performed from the upper estuary in the Cam River (position A, Fig. 1a) to the Nam Trieu mouth (position B, Fig. 1a) or the reverse, in ~3–4 h each. Velocity profiles were measured continuously with a 600 kHz acoustic Doppler current profiler (ADCP RDI Workhorse in bottom tracking mode) configured for a 0.3 m bin size. At each station, depth profiles of water temperature, salinity and turbidity were measured by a Compact-CTD (ASTD687, Alec Electronics Co. (Nishinomiya, Japan), now released by JFE Advantech Co. (Nishinomiya, Japan) as Rinko-Profiler); depth profiles of floc size distribution and concentration were measured using an in situ laser scattering and

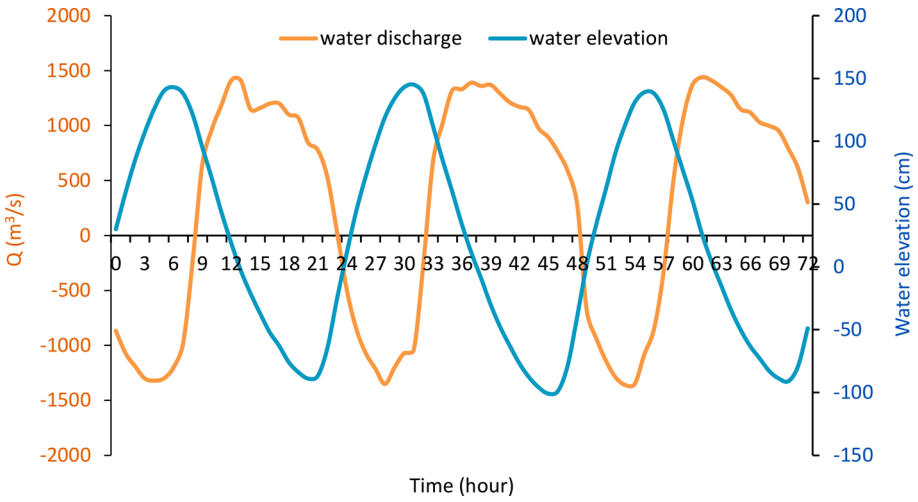

Fig. 2. Hourly water level and water flow at Cua Cam Station (point C in Fig. 1a) in dry season and at spring tide (10–13 January 2016). The water flow is composed of the "mean river discharge" and the "residual flow" which results from the interaction between the tides (and the induced flows) and the river.

transmissometry instrument with a 90% path reduction module (LISST-100X, Sequoia Scientific Inc. (Bellevue, WA, USA); e.g., Traykovski et al., 1999; Agrawal and Pottsmith, 2000). The type-B LISST provided volumetric particulate concentrations in 32 logarithmically spaced size classes ranging from 1.25 to 250 μm and attenuation at $\lambda = 660$ nm. In order to study the relationship between turbidity and SPM concentration, water samples were collected using a Niskin bottle at each station 1.5 m below the surface, from which we measured SPM concentrations and turbidity, measured onboard using a Hach 2100Q turbidimeter. Where possible, we tried to start a transect 1 to 1.5 h before high tide or low tide, in order to consider all measurements as coincident (or quasi-simultaneous). In relation to a full tidal cycle (here ~24 h), we therefore considered that all measurements in a transect were made at approximately the same tidal state (high tide, low tide, early ebb, late ebb, mid-flood etc.).

Data at the hydrographic station of the Cam River (position Cua Cam Station, Fig. 1a), which were provided by the National Hydro-Meteorological Service (NHMS), are also used in this study. They include hourly flow rate and mean SPM concentration (each day, averaged values during "flood tide" and "ebb tide" in the sense of rising water level and decreasing water level, respectively). These data were measured and calculated according to the standard 94 TCN17-99 of the Vietnam Meteorological Hydrological Administration, which is applied in every gauging station in Vietnam, using the same protocol. The hourly flow rate was deduced from the water depth using rating curves that are regularly calibrated (several times a month) using ADCPs at the station. The data were quality-controlled and provided by the Hydrometeorological Data Center. From these values, we calculated the daily water fluxes flowing upward Q_- and downward Q_+, and the daily fluxes of suspended sediment flowing upward Q_{s-} and downward Q_{s+}. The instantaneous flow measured at the station is composed of the "mean river discharge" and the "residual flow" which results from the interaction between the tides (and the induced flows) and the river. The mean river and sediment discharges were estimated as the averages of net flows of water ($Q = Q_+ + Q_-$) and of suspended sediment ($Q_s = Q_{s+} + Q_{s-}$) over 2–4 tidal cycles around spring tides, during the days of surveys. The discharge-weighted suspended sediment concentration was defined as SPM* $= Q_s / Q$ (like in Meybeck et al., 2003; Achite and Ouillon, 2007). At the Hon Dau station in Hon Dau Island (position C, Fig. 1a), data include rainfall (daily), wind (every 6 h) and water elevation (every hour).

3.2. Data processing

3.2.1. SPM concentration and the ratio organic to inorganic matter in the solids of flocs

Suspended particulate matter concentration was determined by filtering about 100–150 mL per sample through pre-weighed polycarbonate Nuclepore filters (porosity 0.4 μm). Filters were rinsed three times with 5.0 mL of distilled water, dried for 24 h at 75 °C in an oven, and then stored in a desiccator until weighing on a high-precision electrobalance (Duy Vinh et al., 2018).

The same process was also applied at selected stations with GF/F filters (porosity 0.7 μm). The sediment concentration after drying 24 h at 75 °C provided the total SPM concentration, which includes organic and inorganic matter. After burning the filter at 450 °C during 2 h, all the organics had been removed and the particulate inorganic matter (PIM) concentration was measured. The difference between the total SPM and PIM provided the particulate organic matter (POM) concentration and thus the ratio of organic to inorganic matter within the solid part of the flocs POM/PIM (Duy Vinh et al., 2018).

3.2.2. SPM volume concentration (SPMVC) and particle size distribution (PSD)

The distribution of volume concentration of particles given by LISST-100X is discretized over 32 size classes. Their sum is providing the SPM volume concentration (SPMVC). However, particles less than the smallest size class or bigger than the largest size class affect the measurements in the spectrum (Traykovski et al., 1999; Agrawal and Pottsmith, 2000; Mikkelsen et al., 2005; Jouon et al., 2008; Andrews et al., 2010; Graham et al., 2012; Fettweis and Baeye, 2015; Many et al., 2016; Pinet et al., 2017). Duy Vinh et al. (2018) followed the recommendation of former authors to remove the first and last classes for calculating the general slope of the particle size distribution and the median apparent diameter D_{50}. In this study based on data between class #2 and class #31, D_{50} was thus calculated as the diameter corresponding to 50% of the cumulative volume concentration of aggregates between 1.48 and 212 μm.

The number of particles of each class, $N(D)$, was calculated from the volumetric particle size distribution (PSD) assuming spherical particles in the assemblage, after a normalization by the width of each logarithmically spaced size bin (Jouon et al., 2008). The more often, a power law relationship can be proposed between N and D following:

$$N(D) = aD^{-j} \quad (1)$$

where a is a coefficient (in number of particles L^{-1} μm^{-1}), D is the

diameter of aggregates and j is the dimensionless exponent, also referred to as the particle size distribution slope or the Junge parameter (Bader, 1970; Jackson et al., 1997). j provides information on the relative concentration of small to large particles: the steeper the slope, the greater proportion of smaller particles and the flatter the slope, the greater proportion of larger particles. Furthermore, j can be estimated from multispectral satellite data of ocean colour through the particulate beam attenuation (Boss et al., 2001) or the particulate backscattering coefficient (Babin et al., 2003).

After skipping the measurements of the first class (<1.48 μm) and the last class (>212 μm) of particle sizes, the grain size range was analyzed through some groups: over the whole particle size range (1.48–212 μm), the fine particle size group (1.48–17.7 μm), the medium particle size group (17.7–92.6 μm), and the coarse particle size group (92.6–212 μm). The classes were defined from our measurements to separate the two extreme peaks (around 3.4 μm and 120–140 μm) from the intermediate peaks around 25 or 45 μm. Other groups may have been considered (e.g., Winterwerp, 1998). The purpose of the groups here is only to illustrate the transfer of particles amongst them during the tidal cycle inferred by flocculation/disaggregation and/or sedimentation/erosion.

3.2.3. Excess of density, settling velocity of flocs and fractal dimension

Settling velocity of flocs, w_s, is the sinking velocity of a floc in still water, which may be reduced by the presence of other flocs that cause hindered settling (Winterwerp, 1998, 2001, 2006). In this study, w_s was calculated from the Stokes formula (Stokes, 1851):

$$w_s = \frac{1}{18\mu}\Delta\rho_f g D^2 \tag{2}$$

where μ is the dynamic viscosity of water, $\Delta\rho_f$ is the excess of density of flocs given by $\Delta\rho_f = \rho_f - \rho$, ρ is the water density, ρ_f is the floc density and g the gravitational acceleration constant. The bulk excess of density of flocs $\Delta\rho_f$ of diameter D_{50} was either calculated at the points where the weight and volume suspended sediment concentrations have been measured (method A), or estimated from the available data and the formulas proposed by Kranenburg (1994) and Maggi (2009) (method B). Both methods are hereafter described.

Method A: at the stations where SPM, SPMVC and ρ were measured, the bulk $\Delta\rho_f$ was calculated under the assumption that flocs were made of particles (subscript p) and water (subscript w), and that their relative component of minerals and organic particles was known. In that case:

$$\frac{\mathrm{SPM}}{\mathrm{SPMVC}} = \frac{M_p}{V_p + V_w} \tag{3}$$

where M_p is the mass concentration of flocs, determined from filtration, $(V_p + V_w)$ is the volume of flocs measured by the LISST. If we note ω the ratio of particulate inorganic matter concentration (PIM, determined by loss of ignition of GF/F filters) to the particulate organic matter concentration (POM), the density of the particulate component of flocs ρ_p was calculated following:

$$\rho_p = \frac{M_p}{V_p} = \omega\,\rho_s + (1-\omega)\rho_o \tag{4}$$

where ρ_s is the density of minerals in the flocs (hereafter considered to be 2650 kg m^{-3}) and ρ_o is the density of organic matter (hereafter considered to be 1100 kg m^{-3}, like Maerz et al., 2016). Finally, at these stations, the measured excess of density was obtained by:

$$\Delta\rho_f = \frac{\mathrm{SPM}}{\mathrm{SPMVC}}\left(1 - \frac{\rho}{\rho_p}\right) \tag{5}$$

If SPM, ρ and ρ_p are expressed in g m^{-3} and SPMVC in μL L^{-1}, $\Delta\rho_f$ is expressed in g mL^{-1} and must be multiplied by 1000 to provide a value in g L^{-1} (or kg m^{-3}). This formula, combined with Eq. (2), provided the bulk w_s values from measurements.

Method B: where SPM was not measured but inferred from turbidity, $\Delta\rho_f$ can be estimated using the fractal description of flocs. Kranenburg (1994) derived the excess floc density $\Delta\rho_f$ of a floc composed of primary particles of diameter D_p and density ρ_p, with fractal dimension d_f:

$$\Delta\rho_f = (\rho_p - \rho)\left(\frac{D_p}{D}\right)^{3-d_f} \tag{6}$$

Maggi (2009) adapted this formula to the case of a floc composed of mineral and organic particles with density ρ_s and ρ_0, respectively, as follows:

$$\Delta\rho_f = [(\omega\rho_s + (1-\omega)\rho_0) - \rho]\left(\frac{D_p}{D}\right)^{3-d_f} \tag{7}$$

which finally gives:

$$w_s = \frac{1}{18\mu}(\omega\Delta\rho_s + (1-\omega)\Delta\rho_0)\,g D_p^{3-d_f} D^{d_f-1} \tag{8}$$

This formula was used to either to estimate the settling velocity of flocs (Kranenburg, 1994; Maggi, 2009; Maerz et al., 2016; van der Lee et al., 2009), or to estimate the fractal dimension d_f where w_s has been determined from measurements by method A. To estimate the bulk w_s of flocs of diameter D_{50}, this relationship was applied with $D_p = 4$ μm (following Fettweis (2008): $D_p = 1.1$ μm in the ETM, 2.1 μm at the edge of ETM and 7.2 μm offshore), $\rho_s = 2650$ kg m^{-3} and $\rho_0 = 1100$ kg m^{-3}, like Maerz et al. (2016) did, and $d_f = 2$ as suggested by Winterwerp (1998). Averaged measured values of ω were considered for the application: $\omega = 0.89$ at flood tide, 0.85 at high and low tides, 0.91 at ebb tide in May 2015 (Duy Vinh et al., 2018), $\omega = 0.91$ at flood tide and 0.92 at ebb tide in September 2015; and $\omega = 0.9$ at ebb tide and 0.92 at ebb-low tide in January 2016. At stations where SPM, SPMVC and ρ were measured, we considered that the bulk $\Delta\rho_f$ provided by eq. (5) was correct, as well as D supposed to be worth D_{50} derived from the LISST measurements. The model of $\Delta\rho_f$ (eq. 7) was then used to estimate the d_f value, considering the bulk measured $\Delta\rho_f$ and under the assumption $D_p = 4$ μm.

3.2.4. Richardson number

The gradient Richardson number, Ri, has largely been used as a criterion for assessing the stability of stratified shear flow through energy consideration (Miles, 1986). It is calculated from the data of ADCP and CTD, following:

$$Ri = \frac{-g\frac{\partial\rho}{\partial z}}{\rho\left(\left(\frac{\partial u}{\partial z}\right)^2 + \left(\frac{\partial v}{\partial z}\right)^2\right)} \tag{10}$$

where u, v are velocity components (m s^{-1}) and ρ the local density of water including the sediment concentration.

3.2.5. Simpson parameter

To quantitatively analyze the physical mechanisms contributing to mixing and stratification in an estuary, Simpson et al. (1978) introduced the potential energy anomaly (Φ), which represents the mechanical energy (in J m^{-3}) required to bring about complete mixing of the water column, given by:

$$\Phi = \frac{1}{D}\int_{-H}^{0} gz(\overline{\rho} - \rho)dz \tag{11}$$

where $\overline{\rho}$ is the depth-mean density.

4. Results

4.1. Hydrosedimentary forcing

As expected, the average river discharge at the Cua Cam station (location in Fig. 1-a; see the variation of the hourly flow there in the dry season in Fig. 2) was maximum in flood period season (783 $m^3\ s^{-1}$ on average from 23 to 25 September 2015), minimum in low-flow season (297 $m^3\ s^{-1}$ on 11–12 January 2016) and intermediate at the beginning of the wet period (459 $m^3\ s^{-1}$, 10–13 May 2015) (Table 1). The standard deviation σ_Q of the hourly flow rate and the average inflow per day Q_- were seen to decrease with increasing river discharge (Table 1).

Interestingly, the discharge-weighted suspended sediment concentration SPM* was higher in dry season (99.9 mg L^{-1}) than in wet season (45.0 mg L^{-1}), with an intermediate value in early wet season (65.2 mg L^{-1}). This evolution is the same for the concentrations averaged over the flood or ebb tides, which are similar at +/− 20% at each season (Table 1). Even if the upward flux of water is always much less than the downward flux, the upward flux of suspended sediment in dry season (-3.37×10^3 tons day^{-1}) is very close to the downward flux of suspended sediment in early wet (3.72×10^3 tons day^{-1}) or wet (3.19×10^3 tons day^{-1}) season. The highest value of sediment supply from the sea to the estuary during flood tide in dry season may either be explained by a higher tidal pumping, induced by a lower freshwater discharge, and/or indicate that the ETM could extend further upstream in dry season, up to the Cua Cam hydrologic station, while it is located further offshore in wet season.

Another important feature of the seasonal variations is that the net flux of suspended sediment Q_s is similar in dry (2.57×10^3 tons day^{-1}) and early wet (2.59×10^3 tons day^{-1}) seasons, the lowest river flow in dry season being counterbalanced by a higher SPM*. However, these values remain lower than the suspended sediment discharge in wet season (3.05×10^3 tons day^{-1}) (Table 1).

In the Cam-Nam Trieu estuary, our measurements showed quasi-linear relationships between measured turbidity and SPM concentrations. These relationships (see Fig. A1), which provided the best determination coefficient between turbidity (in FTU) and SPM concentrations (in mg L^{-1}), were used to estimate the SPM profiles from the measured turbidity profiles. Nevertheless, since turbidity was measured from surface to the bottom at each station and SPM only at two or three points (surface, 1.5 m below the surface and sometimes at a greater depth), we prefer to show hereafter the original, unbiased turbidity data, which do not incorporate the uncertainty of the Turb-SPM conversion, than SPM concentrations.

By definition, ETMs are estuarine areas where turbidity (or sediment load) is the highest. Turbidity of ETMs was found to be higher in early flood period (> 200 FTU corresponding to >140 mg L^{-1} in their core, and ~150 FTU or ~100 mg L^{-1} at their edge) than later during the wet season (> 130 FTU or >270 mg L^{-1} in their core and 60 FTU or ~120 mg L^{-1} at their edge). The highest turbidity and sediment load in ETMs were measured in dry season (>300 FTU or ~235 mg L^{-1} in their core and 150 FTU or ~107 mg L^{-1} at their edge).

4.2. Variations of ETM patterns and aggregate characteristics along transects

Five transects were performed in wet season (Sept. 23–25, 2015) and four in dry season (January 11–12, 2016). A selection of these transects are presented from Figs. 3 to 6. They show a general configuration of ETM with two parts in wet season (Figs. 3a and 4a) and dry season (Figs. 5a and 6a), in accordance with the configuration in early wet season (Duy Vinh et al., 2018).

To support a detailed analysis of their spatial and temporal variability at seasonal and tidal scales, Table 2 reports the length and ranges of turbidity and salinity of the two parts of the ETM, and characteristic parameters at selected stations: Simpson parameter (from eq. 11); depth-averaged S, Turbidity, D_{50}, w_s and J values (J being calculated over the whole size range 1.48–212 μm;w_s using Method B).

Unfortunately, we did not make measurements at each tidal stage and each season. This restriction was due to the fact that the tide is diurnal in this area, and that it was impossible to make measurements there at night within the Haiphong harbor, with a lot of cargos moving back and forth along the main channel. That is why, for example, we could only make measurements at high tide or during ebb in the dry season, since low tide and flood tide occurred at night.

The ranges and along-transect averaged values of aggregate parameters either measured at sub-surface (SPM, SPMVC, $\Delta\rho_f$) or calculated from sub-surface measurements (D_{50}, d_f, w_s) during the three field surveys are given in Table 3 per season and at different tidal phases. w_s values derived from Method A, without any assumption on the diameter of primary particles.

4.2.1. In the wet season

In the wet season, the longitudinal profiles of turbidity showed at high tide the same structure than in early wet season, with an upper ETM developing up to the surface and a maximum value above 80 FTU and a lower ETM restricted to the bottom layer (< 4 m from the bottom) with a local turbidity above 140 FTU (Transect 5, Fig. 3a). The upper ETM started at salinity ~0.1 psu and ended around 2–3 psu, and developed over well mixed waters (Fig. 3b). Its length was around 4 km. The lower ETM developed over stratified waters at higher salinity around 3–10 psu, near the bottom, downstream to an intermediate zone of lower turbidity of around 4 km length.

During the flood tide on September 24, 2015 (Transect 3, Fig. 4), only one maximum of turbidity was measured, above 130 FTU, in well mixed waters and salinity between ~0.1 psu and 2–3 psu as well. The salinity at the river mouth was lower during flood tide (< 5 psu, Fig. 4b) than during high tide (around 10 psu, Fig. 3b). If the lower ETM existed at flood tide on September 24, 2015, it should develop further offshore than the river mouth, in the Bay.

D_{50} values along river transects varied between 30 and 60 μm at high tides (Fig. 3c) and 40–80 μm during flood tides (Fig. 4c). At high tide, the depth-averaged D_{50} was the smallest in the riverine estuary (at salinity <0.1 psu) and slightly increased in the upper ETM (33–47 μm), lower than the mean of whole transect (42.7 μm, Fig. 3c). The same trend occurred during flood tides: D_{50} was 43.6 μm at the riverine station v239 then slightly increased to 45.0 μm at station v245 in the upper ETM (Table 2), lower than the mean of whole transect (53.5 μm). The largest floc sizes (D_{50} > 60 μm at high tide or 80 μm at flood tide) were observed in the low-turbid zone laying between the upper ETM and the lower ETM, and in the core of the lower ETM at high tides (station v307, Fig. 3 and station v250, Fig. 4). D_{50} at high tide was higher than the average (52.8 μm) in the lower ETM (Table 2). At least, we noticed that D_{50} had highest values from each side of the upper ETM (upstream and

Table 1
Mean values and standard deviation of basic hydrosedimentary parameters at the Cua Cam station during the 3 surveys.

Season	Salinity	Q_{ave} +/− σQ	Q_{max}	Q_{min}	Q_+	Q_-	C_{flood}	C_{ebb}	Q_{s_ave}	Q_{s+}	Q_{s-}	SPM*
	(psu)	($m^3\ s^{-1}$)			($10^6\ m^3\ day^{-1}$)		(mg L^{-1})		(10^3 tons day^{-1})			(mg L^{-1})
Early wet season	2.7 ± 4.3	459 ± 836	1490	−1210	57.35	−17.66	70.7 ± 25.6	66.1 ± 22.4	2.59	3.72	−1.14	65.2
Wet season	2.5 ± 3.1	783 ± 643	1540	−339	70.45	−2.76	50.0 ± 4.4	39.1 ± 13.0	3.05	3.19	−0.12	45.0
Dry season	11.1 ± 6.6	297 ± 1034	1440	−1360	57.25	−31.58	93.6 ± 27.4	107.9 ± 31.1	2.57	5.94	−3.37	99.9

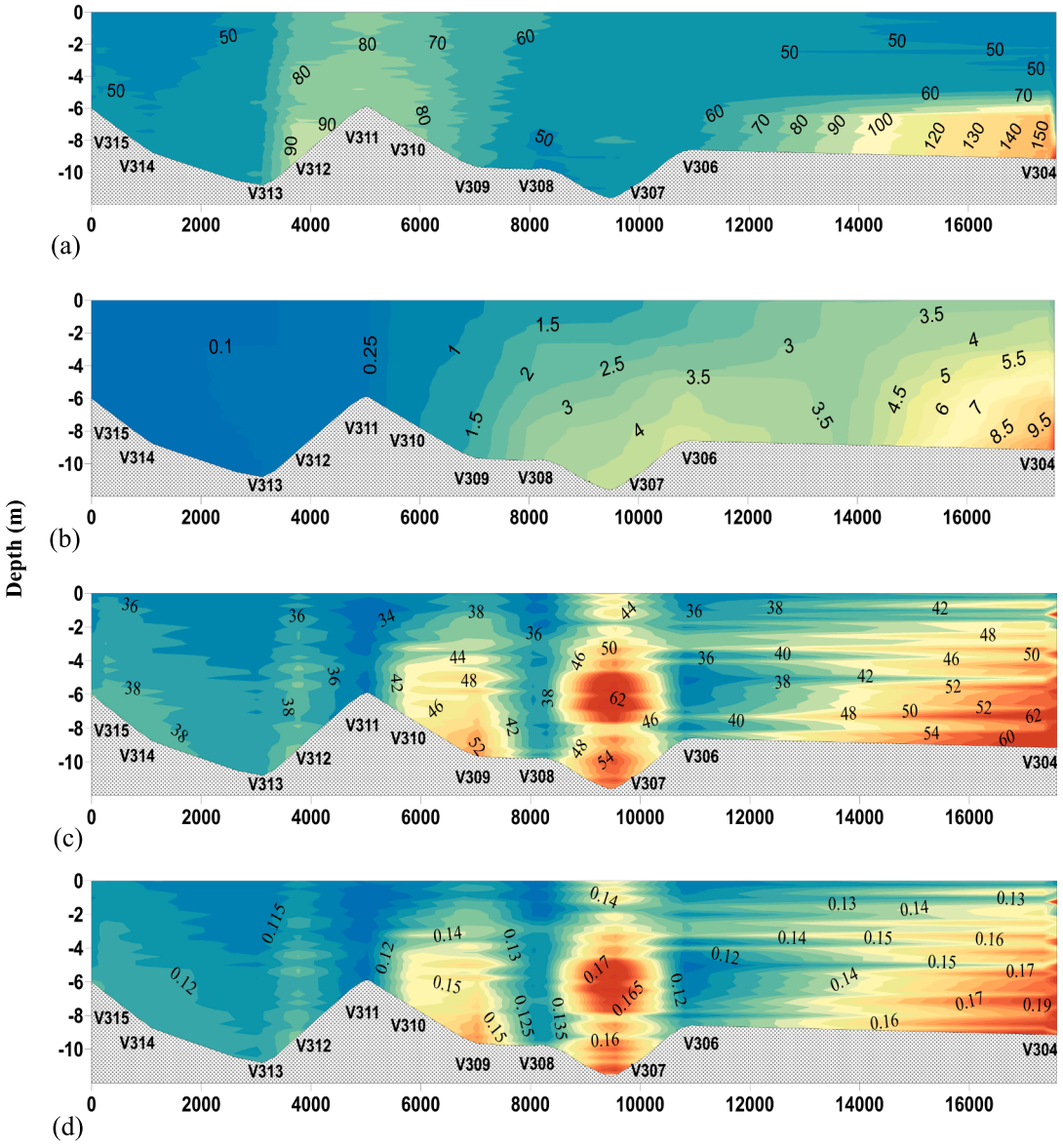

Fig. 3. 2D distributions of parameters along Transect 5 during wet season, high tide (water elevation = 2.8–3.0 m, 25/09/2015). (a) Turbidity (FTU); (b) Salinity (psu); (c) D_{50} calculated over the whole grain size range (1.48–212 μm); (d) Settling velocity of flocs (mm s^{-1}).

downstream) than at its middle, with higher values at its downstream boundary that at its upstream one (v309 vs v312 at high tide, Fig. 3c; v247 vs v244 at flood tide, Fig. 4c).

The spatial distributions of settling velocities were very similar than the distributions of D_{50}. At high tide, the average bulk settling velocities of flocs is 0.13 mm s^{-1}. The highest values were observed at the downstream boundary of the upper ETM (up to 0.16 mm s^{-1}, v309), in the low-turbid zone separating the upper and lower ETMs (0.14–0.18 mm s^{-1}, v307), and in the core of the lower ETM (above 0.16 mm s^{-1}, Fig. 3d). During flood tides, the average of w_s values is 0.17 mm s^{-1}. The highest values (0.19–0.25 mm s^{-1}) were measured at the downstream edge of the upper ETM (v247) and in the low-turbid waters downstream the upper ETM (v250) (Fig. 4d) (the lower ETM was not sampled at this time as it was located further offshore).

In the wet season, the PSD slope (j) showed slight variations within the estuary (not shown), in the range 3.0–3.8 at high tide (averaged value: 3.51) and 2.9–3.6 during flood tide (average: 3.38). j was lower in the lower estuary (and near bottom) and higher in the upper estuary (and subsurface layer), which indicates a higher percentage of coarser aggregates seaward. Its depth-averaged value was higher in the upper ETM and lower in the lower ETM than the averaged of transects (Table 2). For both transects, the lowest values of j were observed in the areas of the highest D_{50} and w_s values, in the low-turbid zone between the upper and lower ETM and, at high tide, in the lower ETM.

These two along-transect distributions of aggregate parameters are rather typical of those measured in wet season. The ranges of salinity, turbidity and other parameters are given at selected stations in the upper and lower ETMs for 3 additional transects in Table 2. In the upper ETM, Φ varied from 0.31–0.37 at high tide to 2.74–2.86 at flood tide. In the lower ETM, Φ were above 15 at ebb tide (v229), around 31 at flood tide (v298) and higher than 67 at high tide (v217, v304) (Table 2). We noticed a much larger range during high tide than flood tide. In the upper ETM, the average Ri was 0.17 at high tide and in the range 0.04–0.08 at flood tide. In the lower ETM, the average Ri was higher, showing a higher stability.

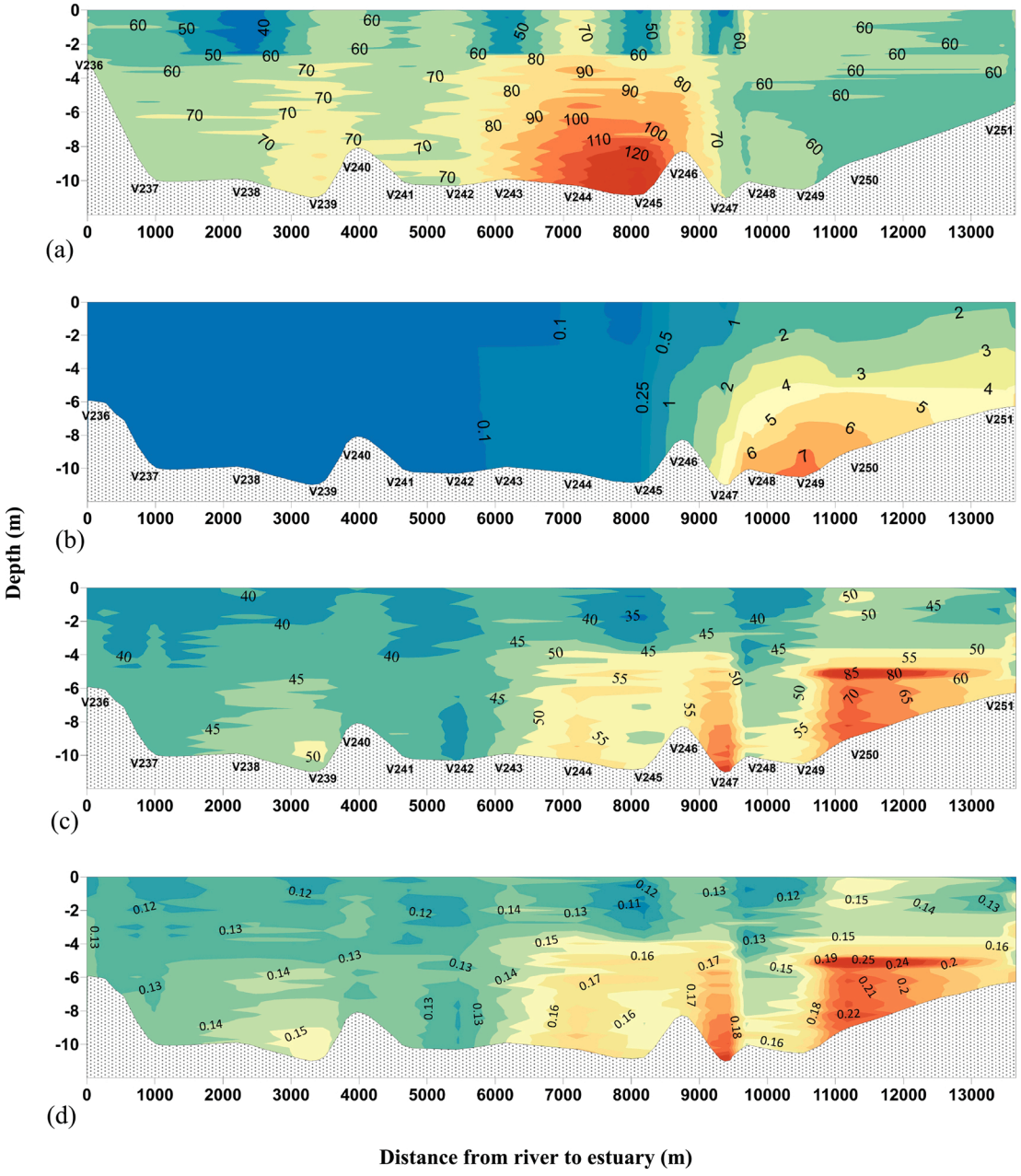

Fig. 4. 2D distributions of parameters along Transect 3 during wet season, flood tide (water elevation = 2.5–3.0 m, 24/09/2015). (a) Turbidity (FTU); (b) Salinity (psu); (c) D_{50} calculated over the whole grain size range (1.48–212 μm); (d) Settling velocity of flocs (mm s^{-1}).

4.2.2. In the dry season

In the dry season, salinity is much higher all along the sampled 14–18 km of the estuary than in the wet season. Contrasted salinity profiles were measured: stratified conditions with 6–8 psu more near the bottom than at the surface (and thus $\Phi > 40$), from 11 to 18 psu upstream to 18–22 psu at the river mouth during early ebb tide (Fig. 5b); and from rather homogeneous salinity profiles upstream (< 1 psu and $\Phi < 2$) to stratified conditions downstream (14–19 psu and $\Phi > 30$) at the river mouth during late ebb tide (Fig. 6b).

The longitudinal profiles of turbidity showed a pronounced upper ETM at late ebb tide with a maximum value above 500 FTU at 2–4 psu (v429) and a lower ETM with a local turbidity reaching 400 FTU at ~10 psu and $\Phi = 10.9$ (v424) (Fig. 6a). Pockets of high values of turbidity (up to 530 FTU) were observed in the bottom and salted layer during early ebb tide in these stratified waters (S > 13 psu, Fig. 5a). No upper ETM was observed in our surveys during early ebb tide or high tide, because salinity was too high at these tidal stages in the sampled area. If an upper ETM existed at these tidal stages in dry season, it should develop further upstream than our upstream limit.

D_{50} values along river transects varied in the ranges 35–75 μm at early ebb tide (Fig. 5c) and 24–68 μm during late ebb tide (Fig. 6c). The largest floc sizes were observed in the lower ETM and at the edges of the upper ETM, the smallest aggregates close to the surface between the two ETMs (Fig. 6c).

As with D_{50}, bulk settling velocities of flocs were slightly higher along estuary at early ebb tide (mean value: 0.16 mm s^{-1}) than at late ebb tide (0.10 mm s^{-1}) (Figs. 5d, 6d, Table 2). In the presence of ETMs (at late ebb tide), the largest settling velocities (w_s > 0.13 mm s^{-1}) were observed at the edges of the upper ETM and in the lower ETM, and the smallest settling velocities (w_s < 0.07 mm s^{-1}) close to the surface between them (Fig. 6c).

We observed a very good covariation of j and D_{50}, with higher

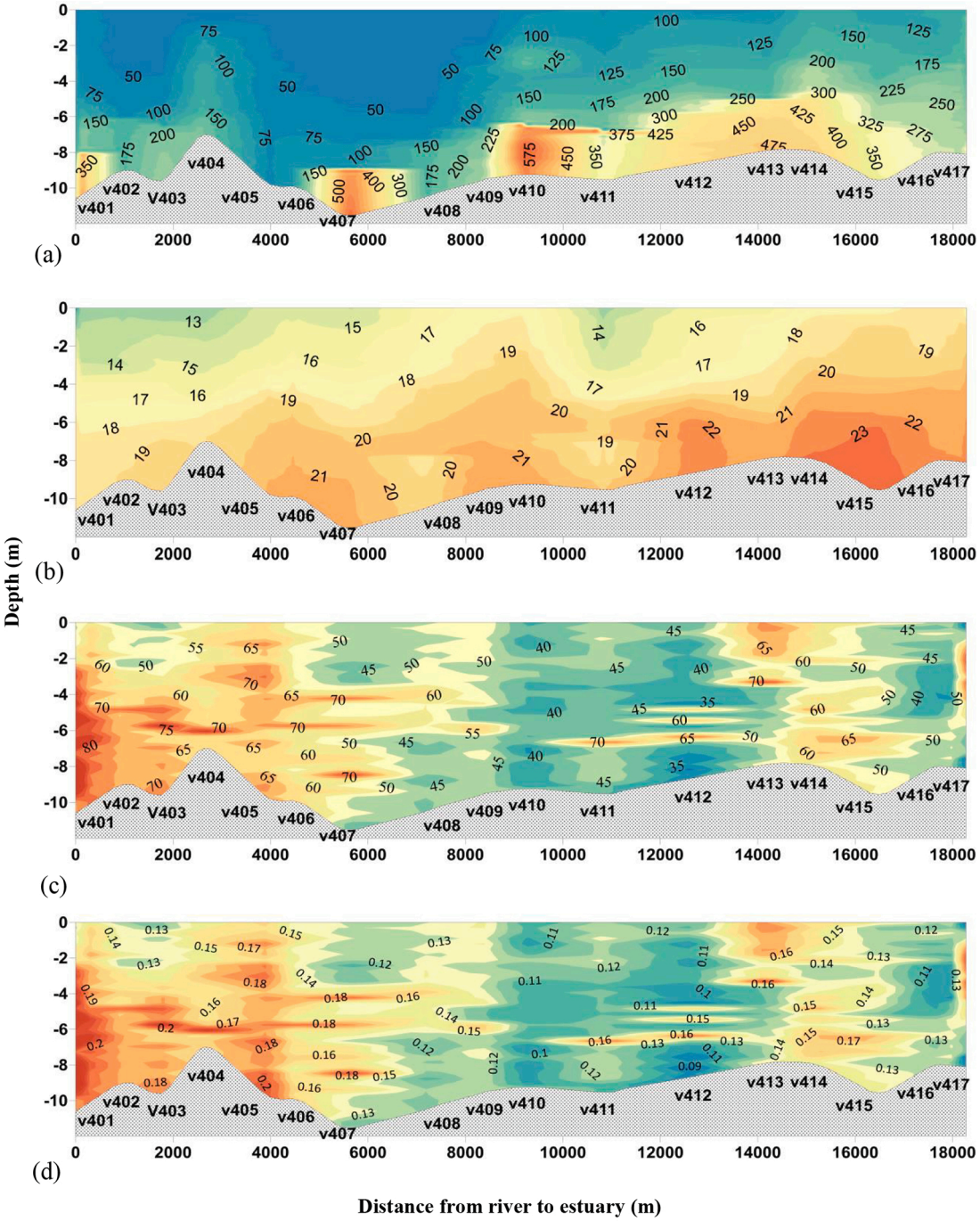

Fig. 5. 2D distributions of parameters along Transect 1 during dry season, early ebb tide (water elevation = 1.3–2.7 m, 11/01/2016). (a) Turbidity (FTU); (b) Salinity (psu); (c) D_{50} calculated over the whole grain size range (1.48–212 μm); (d) Settling velocity of flocs (mm s^{-1}).

proportion of bigger aggregates (smallest *j*-values) where D_{50} is the highest. Their spatial distributions are similar. The PSD slope was in average higher at late ebb tide (3.6) than at early ebb tide (3.1). At late ebb tide, *j* is varying between 3.2 where D_{50} is maximum (~68 μm at v425, in the lower ETM) and 3.8 where D_{50} is minimum (~24 μm near the surface between the two ETM parts).

The Simpson parameter is high all along the transect at early ebb tide (e.g., 48.1 at v414, Table 2), due to the high vertical stratification. At late ebb tide, Φ-values varied between 1.82 (at v430, Transect 2, Fig. 6) and 7.45 (Transect 4, see Table 2) in the upper ETM. Φ was higher than 10 in the lower ETM (see its values at selected typical stations in Table 2: 10.89–13.97 during late ebb tide and >30 in the downstream estuary at high and early ebb tides). *Ri*-values were always lower in the upper ETM (< 0.03 at late ebb tide) than in the lower estuary (> 0.09).

4.3. Tidal and seasonal variations of aggregate parameters

We put in Table 3 the average aggregate parameters during same tidal phases of each survey in sub-surface waters, in order to illustrate their tidal and seasonal variations. Values obtained at ebb tide are interesting since all parameters were measured at this tidal stage during the three surveys. However, caution must be made because of the high variability of parameters in ebb stages, as illustrated in January 2016 when two transects were performed on the same day: one in early ebb

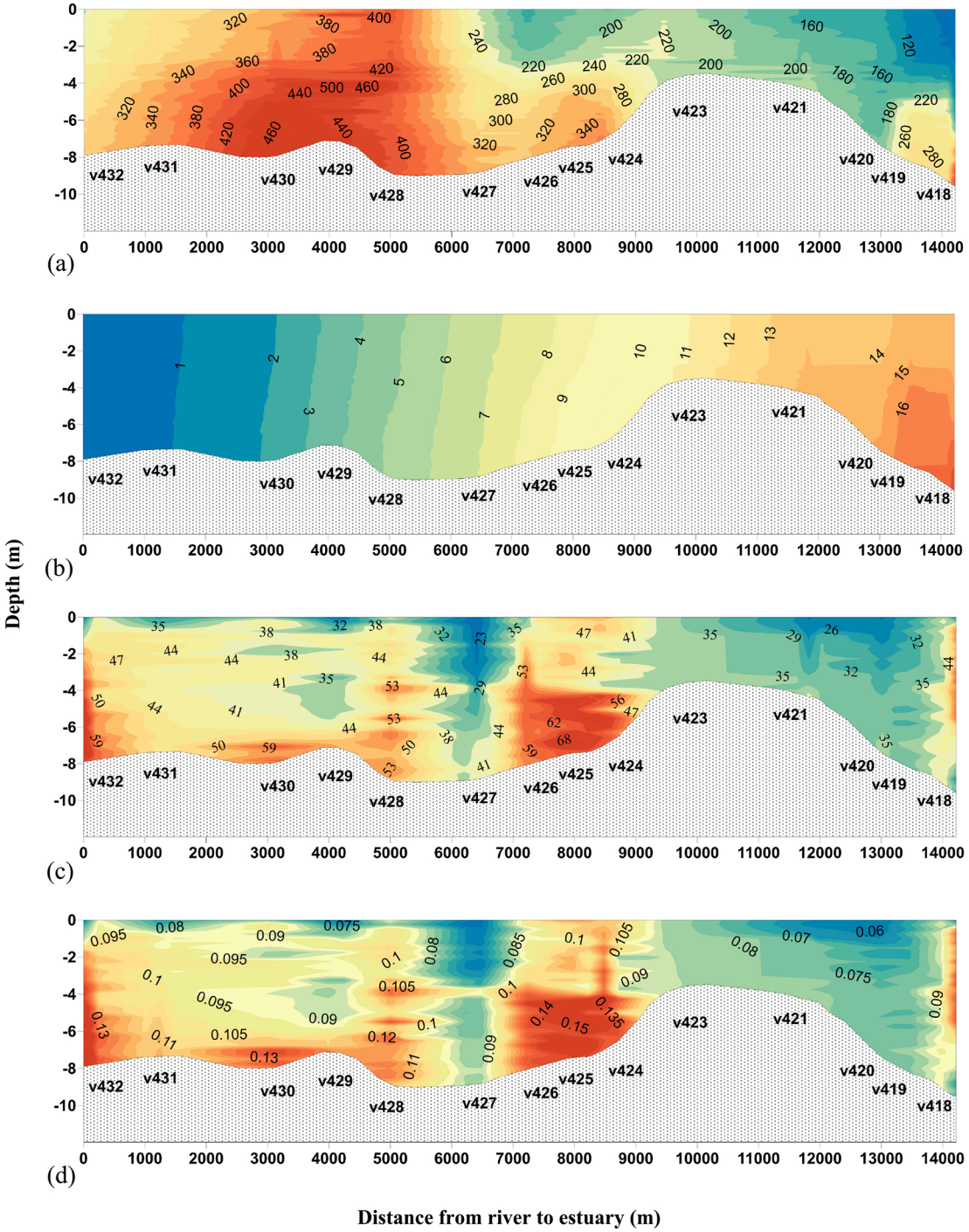

Fig. 6. 2D distributions of parameters along Transect 2 during dry season at late ebb tide (water elevation = 0.5–1.1 m, 11/01/2016). (a) Turbidity (FTU); (b) Salinity (psu); (c) D_{50} calculated over the whole grain size range (1.48–212 μm); (d) Settling velocity of flocs (mm s^{-1}).

stage (Fig. 5), the following in late ebb stage (Fig. 6) (see Table 3): from the early ebb (right after high tide) to late ebb (just before low tide), SPM was multiplied by more than 3, the volume concentration and the excess of density by nearly 2, D_{50} and w_s were divided by more than 2. Unfortunately, no subsurface samples had been performed at the exact high tide during the dry season.

So as to complement the analysis of seasonal variability, we additionally considered the across-transect and depth-averaged values of some major parameters derived from LISST and CTD profiling for all transects and for those performed at high tide only: salinity, D_{50}, w_s and J (Table 4). Transects were performed at ebb tide and high tide during the three surveys, but data collected at high tide will be preferred to those collected at ebb tide to assess their seasonal variations because their variability is much higher during ebb stages than during shorter high tides.

Finally, since Tables 3 and 4 show averaged values, we also considered 99 in situ measurements (23 in the early wet season, 43 in the wet season and 33 in the dry season) of the parameters so as to compare their co-variations. Most of these measurements were performed sub-surface, the other ones within a 5 m-depth surface layer.

In relation with the strong river discharge seasonality, salinity was seen to strongly vary along the transects, e.g. at high tide, from 2.7 psu in

Table 2
Length and ranges of turbidity and salinity of the two parts of ETM, and characteristic parameters at selected stations in the Cam-Nam Trieu estuary, September 2015 and January 2016: Φ, depth-averaged D_{50}, w_s and J values (J was calculated over the whole size range 1.48–212 μm).

Transect	Upper ETM								Lower ETM							
	L (km)	Turb. (NTU)	S (psu)	Station	Φ	D_{50}(μm)	w_s	J	L (km)	Turb. (NTU)	S (psu)	Station	Φ	D_{50}(μm)	w_s	J
Early wet season (May 10–13, 2015)																
1 Flood tide	7	100–250	0.13–0.35	v6	0.98	71.73	0.28	3.34	(1)	125–300	1–(4)	v1	57.12	56.85	0.25	3.51
2 Low tide	4	200–300	0.15–0.25	v21	0.97	65.50	0.28	3.44	(5)	700–1000	0.5–(1.2)	v24[b]	1.22[b]	74.29	0.32	3.50
3 Flood tide	4	120–450	0.15–0.6	v32	1.83	47.1	0.16	3.66	6	150–900	0.3–10	v30	86.99	50.87	0.17	3.55
4 Low tide	13	120–250	0.1–0.4	v46	0.74	81.10	0.39	3.27	(2)	150–310	0.4–(1.0)	v62[b]	3.06[b]	68.14	0.32	3.55
5 High tide	5	100–120	0.2–1	v72	2.05	54.20	0.12	3.55	6	100–250	6–12	v82	61.62	61.81	0.14	3.25
6 Ebb tide	(6)	120–200	(0.15)–1	v104	1.63	62.93	0.17	3.40	4	100–200	5–15	v95	66.64	56.45	0.15	3.36
Wet season (September 23–25, 2015)																
1 High tide	4.5	70–90	0.1–6	v207	0.37	49.0	0.16	3.49	2.5–3	70–150	8–15	v217	87.48	51.64	0.16	3.21
2 Ebb tide	Not sampled (upper ETM likely located further upstream)[c]								5	100–700	4–9	v229	*15.81*[a]	51.34	0.17	3.50
3 Flood tide	5	60–130	0.1–4	v245	2.86	45.04	0.14	3.60	Not sampled (lower ETM likely located further offshore)							
4 Flood tide	5	75–200	0.1–5	v289	2.74	38.78	0.14	3.74	1–1.5	100–500	5–12	v298	31.05	52.96	0.16	3.18
5 High tide	6	60–85	0.1–4	v311	0.31	33.64	0.11	3.69	(5)	70–150	4-(10)	v304	67.75	53.08	0.17	3.31
Dry season (January 11–12, 2016)																
1 Early ebb tide	Not sampled (upper ETM likely located further upstream)								Not sampled (lower ETM likely located further upstream)							
2 Late ebb tide	10–10.5	180–500	0.1–6	v430	1.82	45.61	0.11	3.65	2	120–400	6–12	v424	10.89	64.42	0.15	3.41
3 High tide	Not sampled (upper ETM likely located further upstream)								Not sampled (lower ETM likely located further upstream)							
4 Late ebb tide	6	110–500	0.1–5	v479	7.45	39.92	0.09	3.70	6.5–7	80–350	5–11	v475	13.97	28.42	0.07	3.76

[a] Station v229 was selected because its highest turbidity value. However, it was not representative of stratification along this transect ($20 < \Phi < 50$), since it has the lowest Φ value.
[b] In these two transects, only the edge of the saltwedge at very low salinity (< 1.2 psu) was sampled, these stations may be not representative of the full downstream ETM.
[c] During this transect, measurements were restricted to only 10 km upstream from the river mouth due to navigation constraints, and only the lower ETM was sampled.

average in wet season to 20.0 psu in dry season (Table 4).

SPM values averaged over the transects follow the same variability than salinity, with their highest values and ranges in the dry season and their lowest ones in the wet season, in agreement with the SPM concentrations measured at Cua Cam station (see Tables 1 and 3). Concerning their tidal variability, in early wet season where all tidal stages were sampled, SPM values were clearly the lowest at high tide, the highest at low tide (4 times its average value at high tide) and intermediate at flood and ebb tides (Table 3). SPMVC values were strongly correlated to SPM ($R^2 = 0.852$, not shown), and showed the same tidal evolution (Table 3).

D_{50} varied from maximum values at low tides to minimum values at high and ebb tides (Table 3). The intertidal variability was very high, as illustrated during the dry season with a strong decrease from early to late ebb tide (Table 3). The depth-averaged D_{50} values at high tide was the lowest in wet season (49.7 μm) and the highest in dry season (61.9 μm), with an intermediate value in early wet season (59.6 μm) (Table 4). They show the same seasonal variations than SPM, SPMVC and $\Delta\rho_f$.

The co-variation of D_{50} and SPM is not straightforward (Fig. 7), and just makes it clear that the D_{50} and SPM ranges (or variability) seemed the lowest in wet season for all tidal stages (Fig. 7a) and at high tide for all seasons (Fig. 7b).

4.3.1. *Excess of density*

Like SPM and D_{50}, the range of variability of bulk sub-surface and along-estuary averaged excess of density $\Delta\rho_f$ seemed the lowest in wet season (45–221 kg m^{-3}) and the highest in dry season (56–595 kg m^{-3}). Its values seem to follow the same variations (Table 3), being the highest in dry season. However, the tidal variability of $\Delta\rho_f$ is strong and may differ from a season to another (Table 3); in dry season, $\Delta\rho_f$ was measured to increase by 88% during ebb tide. Furthermore, we have to remind that we did not sampled at same tidal stages in each season. A higher range of variability in dry season for SPM, D_{50} and $\Delta\rho_f$ values may indicate that ETMs are stronger in dry season than in wet season.

Locally, the variations of $\Delta\rho_f$ followed the ones of SPM in each season (Fig. 8a) and over a tidal cycle (Fig. 8b) but their relative increase or decrease is also affected by the variation of D_{50} (Fig. 9a and b). $\Delta\rho_f$ is seen to increase with increasing SPM (Fig. 8) and to decrease with increasing D_{50} (Fig. 9). The trends (slopes) vary a little amongst seasons and much more amongst tidal stages (see, e.g., Fig. 8b compared to 8a). The tidal variations of SPM likely explain the tidal variations of $\Delta\rho_f$, from the lowest values at high tide to the highest values at low tide (Fig. 8b).

The floc fractal dimension (d_f) calculated from 99 in situ measurements varied from 1.91 to 2.09. Like other parameters, the range of values was slightly higher in the dry season than in the early wet and wet season (Table 3). The seasonal variation of d_f (1.97 in dry season and 2.00 in wet season at ebb tide, Table 3) was lower than its tidal variations (+/−5% around the average value), which are not straightforward. In dry season smaller d_f values at late ebb tide corresponded to much smaller aggregates ($D_{50} = 21.7$ μm) with a higher excess of density ($\Delta\rho_f = 224.5$ kg m^{-3}) than at early ebb tide ($D_{50} = 46.3$ μm, $\Delta\rho_f = 119.2$ kg m^{-3}) (Table 3). The comparison between averaged values of each parameter at early ebb and late ebb in dry season (increase in SPM, SPMVC, $\Delta\rho_f$; decrease in D_{50}, d_f, w_s) is particularly instructive on their high variability at the tidal scale in this season (Table 3).

The depth-average PSD slopes J along the Cam-Nam Trieu estuary increased from dry season (3.13 in average at high tide) to early wet season (3.39) and wet season (3.44) (Table 4, see examples on Fig. 10b). Thus, aggregation seems to be enhanced in dry season and reduced in wet season, and its seasonal variations are the same than d_f. A detailed comparison of the PSDs between wet and dry seasons(see, e.g., Fig. 10a) shows that, at high tide, the proportion of fine aggregates decreased from35.2% to 30.5% in average, and the proportion of coarse aggregates increased from 27.4% to 33.1%.

The bulk settling velocity was calculated from the Stokes

Table 3
Seasonal and tidal variations of aggregate parameters in the Cam-Nam Trieu estuary. Values averaged along the estuary from subsurface sampling and LISST measurements at different tidal phases.

Parameters	Early wet season[a] (May 11–13, 2015)						Wet season[b] (September 23–25, 2015)					Dry season[c] (January 11–12, 2016)				
	Min	Max	Tidal phase				Min	Max	Tidal phase			Min	Max	Tidal phase		
			Flood	High	Ebb	Low			Flood	High	Ebb			Early ebb	Late ebb	Mean ebb
SPM (mg L^{-1})	20.0	257.5	82.37	37.8	42.3	160.8	25.7	128.5	49.5	50.7	73.0	28.7	384.4	64.5	205.9	135.2
SPMVC (µl L^{-1})	176.0	1007.0	316.5	196	187.0	587.0	152.2	709.4	204.2	217.7	296.4	181.9	1166.6	307.2	605.8	456.5
D_{50} (µm)	31.0	81.0	45.9	39.9	37.9	56.0	27.4	71.2	45.9	38.8	39.1	17.6	77.0	46.3	21.7	43.1
$\Delta\rho_f$ (kg m^{-3})	66.6	260.2	156.5	110.6	133.2	169.8	44.8	221.5	146.7	153.2	162.2	55.9	595.1	119.2	224.5	171.8
w_s (mm s^{-1})	0.07	0.55	0.18	0.09	0.11	0.29	0.07	0.29	0.17	0.12	0.13	0.03	0.42	0.14	0.06	0.10
d_f	1.93	2.07	2.02	1.97	1.98	2.04	1.92	2.06	2.01	1.99	2.00	1.91	2.09	1.98	1.96	1.97

[a] 23 stations.
[b] 43 stations.
[c] 33 stations.

Table 4
Mean values and standard deviations of salinity and aggregates parameters at each season, calculated separately from all transects and from transects performed at high tide only. The values are averaged over the whole transects, from upstream to downstream and from surface to bottom.

Season	Early wet season		Wet season		Dry season	
Transects considered	All transects	High tide	All transects	High tide	All transects	High tide
S (psu)	2.6 ± 4.2	6.6 ± 5.8	2.5 ± 3.1	2.7 ± 3.7	14.8 ± 7.2	20.0 ± 3.8
D_{50} (µm)	59.6 ± 10.9	52.3 ± 6.1	49.6 ± 11.6	49.7 ± 11.7	51.3 ± 13.5	61.9 ± 11.6
w_s (mm s^{-1})	0.21 ± 0.09	0.12 ± 0.01	0.11 ± 0.06	0.11 ± 0.05	0.13 ± 0.04	0.17 ± 0.03
J	3.39 ± 0.11	3.37 ± 0.12	3.44 ± 0.19	3.44 ± 0.20	3.34 ± 0.27	3.13 ± 0.13

relationship, considering D_{50} derived from LISST measurements, by two methods, considering either the measured $\Delta\rho_f$ at stations where water was sampled (method A, Table 3), or the bulk $\Delta\rho_f$ derived from a model based on fractal distribution of aggregates, with $d_f = 2.0$, $D_p = 4.0$ µm, and $D = D_{50}$ along the whole transects (method B, Table 4). The comparison between these two methods at the sampled stations (Fig. 11) shows a good correlation between the measured value and the estimated value based on the model, and indicates that, globally, the model (before adjustment of d_f) tends to overestimate the measured settling velocities up to ~0.12 mm s^{-1}, and to underestimate higher settling velocities. Overestimation occurred mainly in dry season or at low and high tides, underestimation in early wet season, or at ebb and flood tides. In a second step, d_f was adjusted at 99 sampled stations in Method B until it provides the same settling velocity than Method A, considered as the reference.

The bulk settling velocity of aggregates clearly showed to increase with increasing D_{50} (Fig. 12, Tables 3 and 4). It also showed to vary with seasons and tides, but its tidal variations seem to vary a little seasonally. The seasonal and tidal variations are thus not straightforward. Although w_s decreased from early ebb (0.14 mm s^{-1}, Table 3) to late ebb tide (0.06 mm s^{-1}) in dry season, we observed the smallest w_s values at high tide in early wet and wet seasons. Concerning its seasonal variations, at high tides, w_s was higher in dry season (0.17 mm s^{-1} in average, Table 4) than in wet season (0.11 mm s^{-1}, Table 4) with intermediate values in early wet season (0.12 mm s^{-1}, Table 4). It was the reverse at ebb tides, with the highest w_s (0.13 mm s^{-1}) and the smallest in the dry season (0.10 mm s^{-1}) (Table 3, Fig. 12a) but, as the range of variation is higher during ebb than at high tides (Fig. 12b), the seasonal variation is assumed to be more representative at high tides.

Although the power-law regression curve between w_s and SPM was good in early wet season (R^2 = 0.64 through power-law regression curve, not shown), it was very poor in the dry season (R^2 = 0.23) and not significant in the wet season (R^2 = 0.09). Furthermore, while w_s tended to increase with increasing SPM in early wet and wet seasons, it tended to decrease with increasing SPM in dry season.

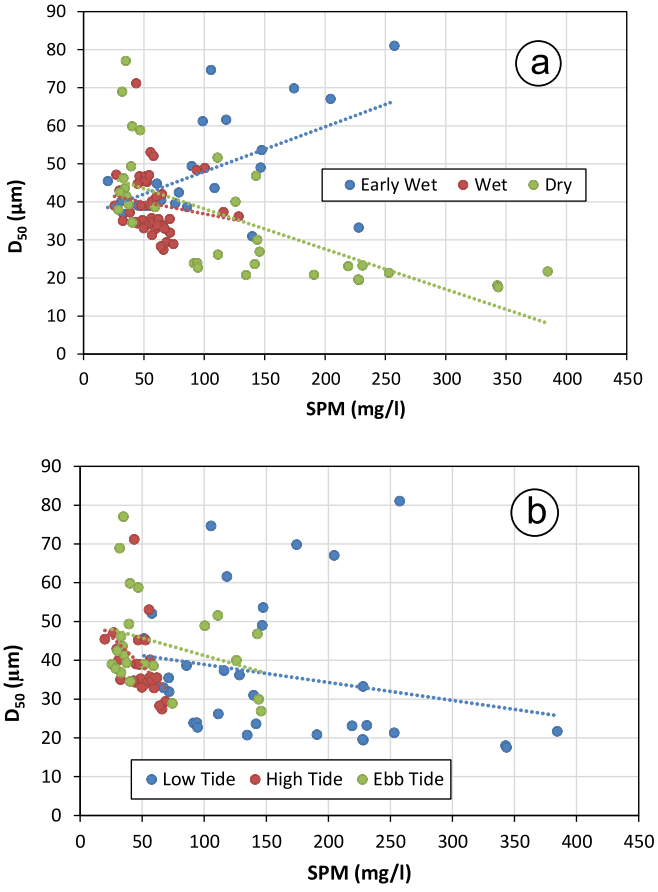

Fig. 7. Sensitivity of D_{50} to SPM volume concentration for 99 samples, May 2015, Sept 2015 and January 2016: (a) seasonal trends, (b) tidal trends.

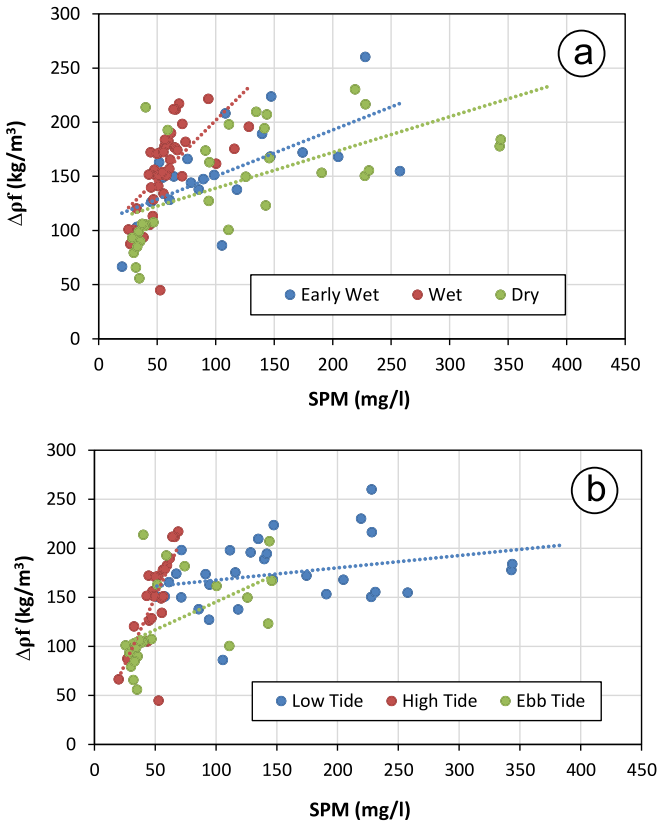

Fig. 8. Covariation of measured values of bulk excess of density $\Delta\rho_f$ and SPM for 99 samples, May 2015, Sept 2015 and January 2016

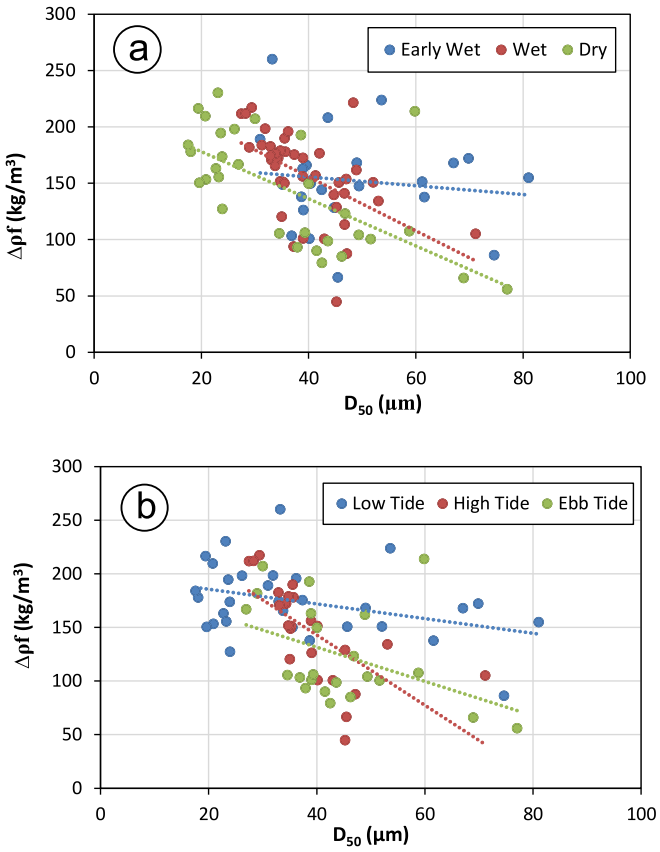

Fig. 9. Covariation of measured values of bulk excess of density $\Delta\rho_f$ and D_{50} for 99 samples, May 2015, Sept 2015 and January 2016.

Several reasons may explain the high difference between the average bulk w_s along the transects at different seasons and tides, like different ranges of parameters. We should also consider that the ETM moved seasonally, and that from the river mouth to 18 km upstream we did not sample waters in the same portions of estuary from a season to another. In dry season, the sampling area corresponded with the ETM at late ebb only (Fig. 6), while it corresponded to the river plume (at higher salinity, in partially mixed waters, with higher D_{50} values) at early ebb (Fig. 5). We thus need to analyze the seasonal variations of the ETM: this is the purpose of next subsection. And we suggest a future peculiar study dedicated on the apparent lowest D_{50} and w_s values in dry season at late ebb or around low tide, since this is the period of the tidal cycle and of the year where sedimentation in the estuary is assumed to be the highest, and thus the sediment balance is very sensitive to the combination of seasonal and tidal variations of settling velocities.

4.4. *Seasonal variation of ETM patterns and characteristics*

The two parts of ETM – an upstream part in well mixed waters and a downstream one restricted to the bottom boundary layer – were observed at each season. However, they showed special patterns and seasonal characteristics.

In the wet season, the lower ETM was much bigger than the upper ETM. The upper and lower ETMs seemed to be at longer distance from each other than in the early wet season. They look almost disconnected from each other. At high tide (Transect 5, Fig. 3 + Transect 1, not shown), the upper ETM developed at salinities in the range 0.1–4 psu, and the lower ETM at salinities 3–11 psu near the bottom, with an intermediate zone of lower turbidity of ~4 km length.

In the dry season, the limit of stratification was observed at Simpson values around 10. This appears to be the lower limit of the upper ETM. The upper ETM was much bigger than the lower ETM. The upper ETM developed at salinity up to 3–6 psu at surface, and the lower ETM up to 12–15 psu near the bottom.

The seasonal and tidal variations of turbidity within the full ETM seem clear and consistent with all transects. In early wet and wet season, the highest turbidity values are located over large areas in the lower part of ETM (up to 1000 NTU at low tide and up to 300 NTU at high tide). They are restrited to a bottom layer no more than half the height of the water column. In the upper ETM, the maximum turbidity is 250–300 NTU at low tide and around 120 NTU at high tide near the bottom. Similar distributions were observed in early wet and wet season, with slightly lower values in wet season than in early wet season. In the dry season, the turbidity distribution is much different, with higher turbidity in the upper part of ETM than in the lower part. Unfortunatelly, we did not investigate the ETM at high tide (likely developing more upstream than 18 km from the river mouth). However, at late ebb tide, near low tide, we observed two times the same structure with a huge upper ETM (turbidity ranging from 500 NTU near the bottom to 300–400 NTU at the surface) and a smaller and shorter lower ETM with maximum turbidity of 350 NTU (near the bottom). Local pockets of high turbidity were also observed downstream of the lower part of ETM, being mainly restricted to the bottom layer in these highly stratified waters (e.g. from stations v412 to v414, Fig. 5).

An additional seasonal variation seems very clear and consistent from our observations. In early wet and wet season, the upper ETM and lower ETM have either similar lengths (4–5 km) or a longer lower ETM (> 6 km, in early wet season). They are generally spaced by a distance from 1 to 4 km. In dry season, the configuration is very different with a much longer upper ETM (>7 km) and no distance between the two parts of the ETM (see Fig. 6: an upper ETM from upstream down to station v427, which correspond to the maximum of turbidity at surface + a lower ETM between stations v427 and v424 or v423).

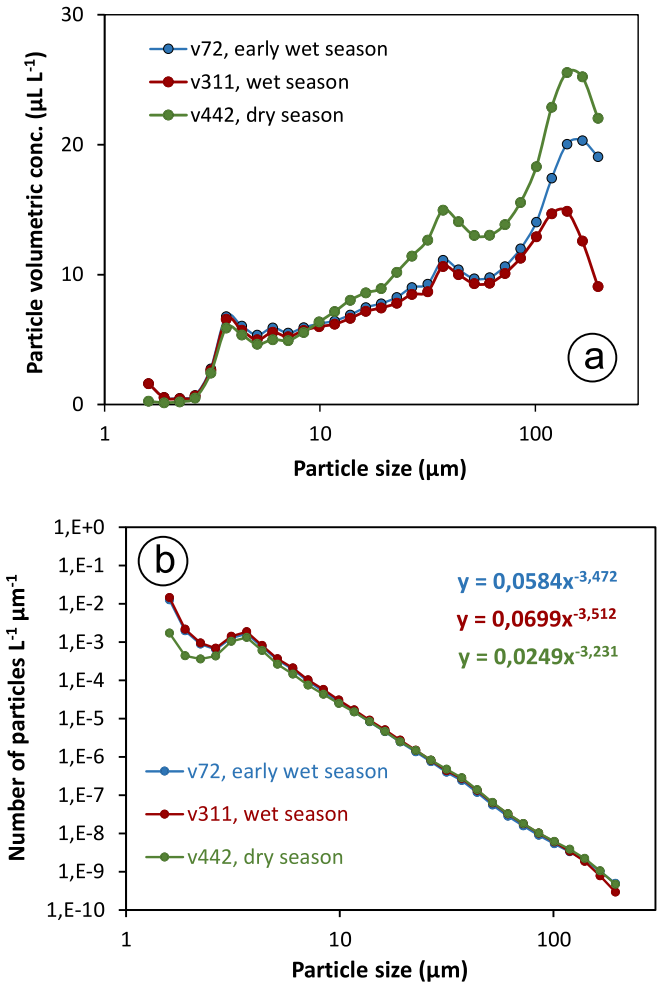

Fig. 10. Example of average Particle Size Distribution (PSD) at high tides at selected stations and different seasons: (a) volumetric distribution along the 32 size classes; (b) log-log representation used to calculate the Junge parameter.

We tried to characterize the boundaries of the upper and lower parts of the ETM from their Simpson parameter and depth-averaged salinity. The upper limit of upper ETMs are characterized by both low salinity (mostly in the range 0.09–0.12 psu) with a median value of 0.105 psu, and low Φ values (in the range 0.2–1.2), with a median value of 0.65 (Fig. 13a). These ranges and median were calculated only in early wet and wet season because the further upstream stations in dry season (at salinity values of 0.3 and 0.6 psu) were downstream of the upper limit of upper ETMs. Fig. 13b shows that the lower limit of the upper ETM in salinity is varying with the season (median values of 7.30 psu in dry season, 1.77 psu in early wet season and 1.27 in wet season), but that the median values of Φ calculated per season are very close (7.0 in early wet season, 8.0 in wet season and 9.4 in dry season). The slightly higher value of Φ in dry season may be associated to the higher turbidity values at this season. To summarize, the upper limit of the upper ETM seems to be driven by salinity, around 0.1 psu, (at Φ-values = 0.65 +/− 0.5) and the lower limit may be driven by the stratification at Simpson parameter around 8 in the range 7–10, at salinity less than 8–10 psu in dry season and 2–3 psu in wet season.

The lower ETM is more difficult to characterize, since we generally measured only one part of it. The maximum of salinity seemed to be around 15 psu from the whole data set. Most of our transects show a salinity range between 5 and 15 but we also observed lower ETM parts (i.e. restricted to the bottom) at lower salinity values (see Table 2). Simpson values were higher than in the upper ETM, most of the time higher than 10.

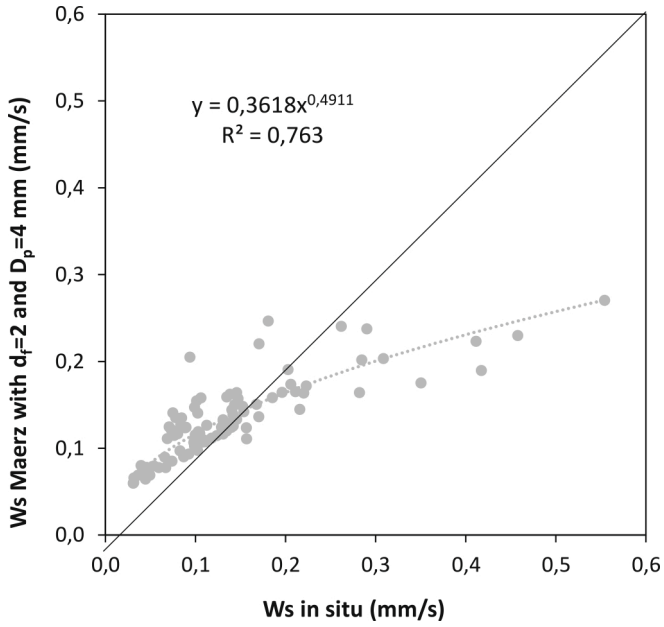

Fig. 11. Comparison between w_s estimates based on a fractal distribution of flocs under the assumption $D_p = 4$ mm and $d_f = 2$ (eq. 8) and w_s derived from the measured $\Delta\rho_f$ (eq. 2 and 5), for 99 samples.

While the upper ETM (which developed over one vertical water column from S=0.1 psu until $\Phi \sim 8$) was clearly separated from the lower ETM in wet season (e.g. Fig. 4), in dry season it was sticking the lower ETM, which developed only near the bottom (Transect 2, Fig. 6 + Transect 4, not shown). The same structure was observed two times in dry season (Transects 2 and 4). One hypothesis to explain the difference between their seasonal distributions is that the longitudinal salinity gradients are much smaller in wet season and thus enable the ETMs to develop over greater length.

At upper ETMs, *Ri* showed seasonal variations between 0.10 in average in wet season and 0.02 in average in dry season, with intermediate values in the early wet season (0.07). The same trend was observed in the lower ETM, with average R_i values between 2.5 in wet season and 0.36 in dry season. We can infer that (1) the density stratification is more stable in the lower ETM than in the upper ETM, and (2) that the density stratification is more stable in wet season than in dry season. However, we must emphasize that the tidal variations of *Ri* are much higher than their seasonal variations.

The depth-average size of aggregates at ETMs varied with seasons (see Table 2). In the wet and dry seasons, average D_{50} values in the upper ETM were similar (41.6 µm in the wet season, and 42.8 µm in the dry season) and smaller than in the lower ETM (52.3 µm in the wet season and 46.8 µm in the dry season). In the early wet season, both values were higher (63.8 µm in upper ETMs and 61.4 µm in lower ETMs).

The depth-average settling velocity of aggregates was shown to decrease from early wet season (0.23 mm s^{-1} in average for both ETMs) to wet season (average 0.15 mm s^{-1}), then to dry season (average 0.11 mm s^{-1}) (Table 2). In the core of ETMs, averaged settling velocities of aggregates were slightly lower in the upper ETMs than in the lower ETMs (0.14 mm s^{-1} compared to 0.17 mm s^{-1} in the wet season, 0.10 mm s^{-1} compared to 0.11 mm s^{-1} in the dry season, Table 2). Reverse variations were observed for the average PSD slopes in the cores of ETMs, with lower values in early wet season (3.45 in average) than in wet season (3.47), and a higher value in dry season (3.63). *J* values were also higher in upper ETMs than in the lower ETMs (3.47 compared to 3.30 in the wet season, 3.63 compared to 3.59 in the dry season, Table 2). We can note that the difference between values in both parts of the ETM is maximum in the wet season.

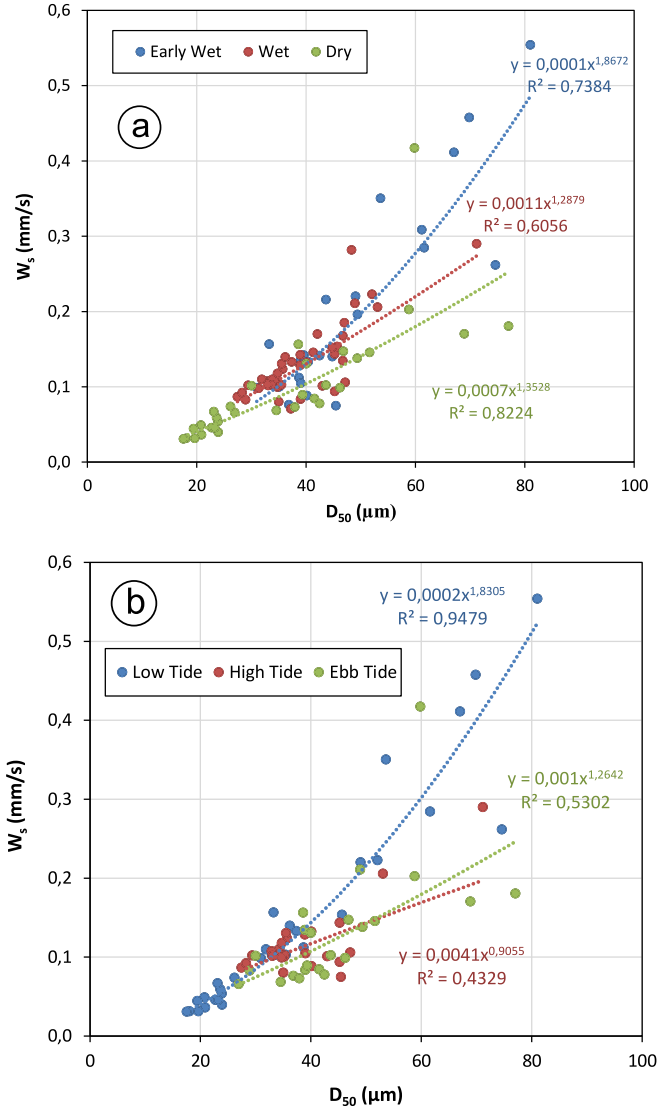

Fig. 12. Sensitivity of w_s to D_{50} for 99 samples, May 2015, Sept 2015 and January 2016: (a) seasonal trends, (b) tidal trends.

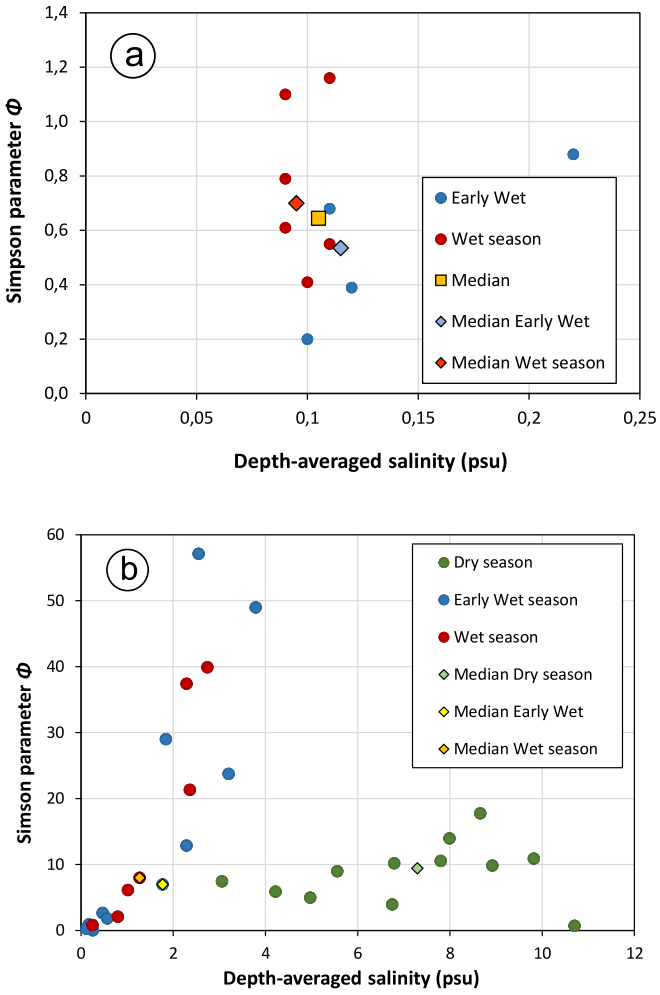

Fig. 13. Simpson parameter and depth-averaged salinity values at stations assumed to be at or near the boundaries of upper ETMs, and their median values: (a) at its upper limit, (b) at its lower limit.

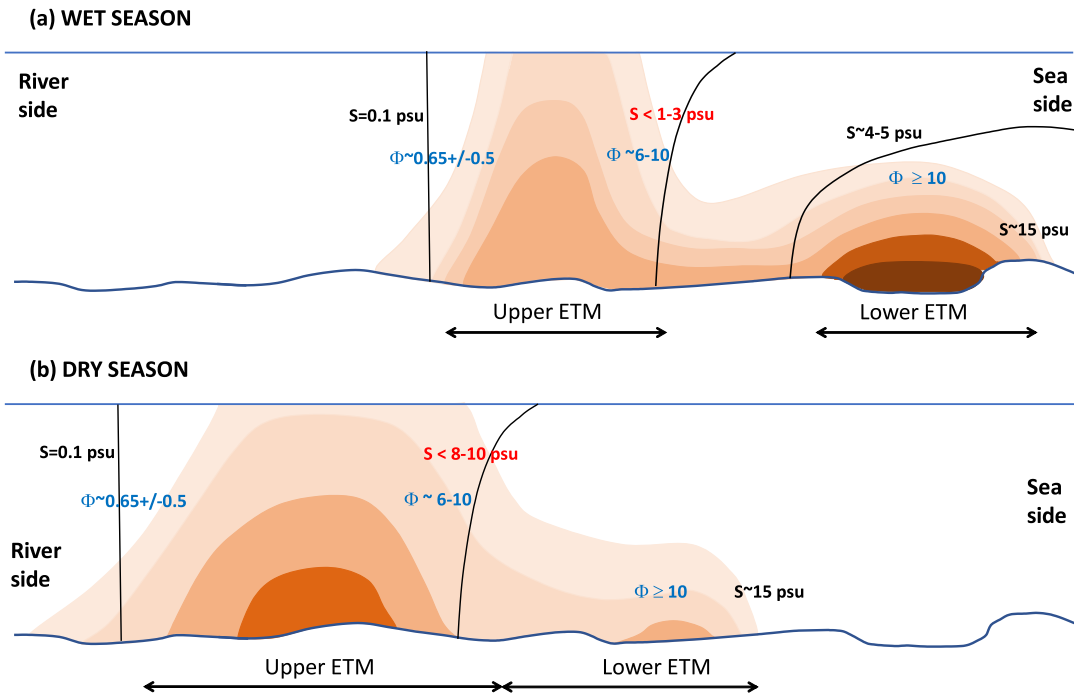

Fig. 14. Seasonal patterns of the ETM in the Cam-Nam Trieu estuary at spring tides (a) in early wet or wet season in May-Sept. 2015 and (b) in dry season, January 2016. Isohaline lines are given in blue (with salinity in psu) and turbidity patterns are showed in brown with darker colour for higher turbidity values. (For interpretation of the references to colour in this figure legend, the reader is referred to the web version of this article.)

5. Discussion

5.1. Seasonal variations of the river discharge at the hydrographic station

The hourly measurements of water flow at the hydrographic Cua Cam station confirmed that the river discharge was increasing from the dry to the wet season, and that the daily volume of inflow Q_- was decreasing with increasing river discharge (from -31.6×10^6 m^3 day^{-1} on 11–12 January 2016 to -2.8×10^6 m^3 day^{-1} on 23–25 September 2015) (Table 1). However, we were surprised to measure the same outflow Q_+ ($\sim 57.3 \times 10^6$ m^3 day^{-1}) for two distinct river flows Q (297 and 459 m^3 s^{-1}) and with the same tidal range (spring tide, i.e. ~2.4 m amplitude) (Table 1). It shows that, for a particular outflow Q_+, the decrease of inflow $Q_- = Q - Q_+$ counterbalanced exactly the increase of river discharge. This process being far from the core of the present paper, it will be described and explain in detail in a future paper.

Water river and sediment supplies from the Red River to the sea have changed after Hoa Binh Dam impoundment (Vinh et al., 2014), resulting in a strong decrease of extreme river flow in the wet season, a higher water discharge in the dry season and a strong decrease in SPM concentration. However, in the RRD estuary and coastal area, the SPM concentration also depends on tidal oscillation (Lefebvre et al., 2012; Vinh and Uu, 2013) and ETM propagation upstream. The ETM moves further upstream in dry season. That may explain why a higher SPM concentration at Cua Cam Station was measured in the dry season than in the wet season, in agreement with the SPM concentration averaged over all samples during each field campaign (124.9 mg L^{-1} in the dry season vs. 59.4 mg L^{-1} in the wet season). The same seasonal variation during spring tides was measured in the Van Uc estuary (whose mouth is ~15 km from Cam-Nam Trieu mouth), with 3–4 times higher SPM values in dry season than in wet season (Piton et al., 2020b). However, we learned in the Van Uc estuary than the reverse occurs at neap tides, with much higher SPM values in the wet season than in the dry season. It is therefore difficult to conclude that the observed variations of concentrations during the 3 campaigns of 2015–2016 were typical and could be generalized to other tidal stages than spring tides.

5.2. Seasonal patterns of ETM

Considering the double structure of the ETM and their respective limits in terms of salinity and stratification (see § 4.4), we can summarize their configuration in the Cam-Nam Trieu estuary in the dry and wet season in Fig. 14. The upper ETM was much bigger and with much higher turbidity values in dry season than in the wet season. The lower ETM showed higher turbidity than the upper ETM in the wet season.

The double structure of the ETM is perfectly consistent with the description of the Gironde estuary by Gibbs et al. (1989): coagulation induced by salinity at low S values (from around 0.1 psu to 1 psu – the "coagulation zone", salinity controlled) with a progressive increase in floc diameter and volume concentration occurs in quite homogeneous waters, forming the upstream part of the ETM; and flocculation is induced by hydrodynamic processes near the null point, the convergence of seaward and landward flows of water (at S values around 4–5 psu in the Gironde), where some stratification develops. Flocs settle in the 5–18 psu and move landward near the bottom towards the null point

Table 5
Variations of transect-averaged aggregate parameters in the Cam-Nam Trieu estuary at tidal scale and at seasonal scale during spring tides. + indicates the highest values, − the lowest ones, and some intermediate values (generally noted =) are mentioned as closest to the highest values (=+) or to the lowest ones (=−).

Aggregate parameters	Tidal variations				Seasonal variations		
	Flood	High	Ebb	Low	Early wet	Wet	Dry
SPM, SPMVC values	=−	−	=+	+	−	=	+
SPM, SPMVC ranges	=	−	=	+	=	−	+
D_{50}	=+	−	=−	+	=	−	+
$\Delta\rho_f$	=	−	=	+	−	=	+
w_s	=+	−	=−	+	=−	−	+
d_f	=+	−	=−	+	=	+	−
J					=+	+	−

area, developing the downstream part of the ETM (see Gibbs et al., 1989, their Fig. 11).

The tidal and seasonal migrations of ETMs towards downstream/upstream locations were already described in the literature (e.g. Allen and Castaing, 1973; Schoellhamer, 2001; Rao et al., 2011). The seasonal motion of the ETM can be further commented. By comparing two campaigns carried out in this estuary, Lefebvre et al. (2012) showed that in the rainy season, the particles brought by the floods are mainly deposited in the coastal zone and at sea, and that some of them return to be deposited in the estuary in the dry season, with a deposition rate in the estuary that is three times higher in the dry season than in the rainy season. The present study shows that the ETM (and therefore the preferential areas of deposition) are located in the dry season around the Haiphong harbor at low tide (Fig. 6), when particles settle. Sedimentation is thus the highest in the harbor area at the period of the year when its rate is maximum (Lefebvre et al., 2012). In the present configuration (and with the present water regulation), Haiphong harbor is the area with the highest turbidity and sediment deposition rate, consistently with the location of mud dredging activities. It is likely that before flows were regulated by dams, the ETM in low flow season (with lower discharge) was located further upstream in the estuary, and therefore the deposition that occurred did not affect siltation and navigability at the harbor as much. This could explain the recent increase in both harbor siltation and dredging activities to maintain the navigability of the main channel (Duy Vinh et al., 2018).

5.3. Variability of aggregate characteristics

The variability of aggregate parameters is known to be high at tidal scale in mesotidal environments, especially at low flow periods, as detailed by Piton et al. (2020b) in the neighboring estuary of the Van Uc River, or as outlined in § 4.3. The present subsection aims at summarizing their variability at tidal and seasonal scales (Table 5) and discussing it with regard to the literature.

The tidal variations of the aggregate parameters (SPM, D_{50}, $\Delta\rho_f$, w_s, d_f) showed to be consistent, with their highest values at low tide, their lowest values at high tide and intermediate values at flood and ebb. A more detailed analysis of our data set showed that for some parameters (D_{50}, w_s, d_f), the "intermediate" values were slightly higher at flood than the ebb (Table 5), and the reverse was observed for SPM. Regarding the seasonal variations, the dry season is clearly characterized by extreme values, the highest ones for SPM, D_{50}, $\Delta\rho_f$ and w_s, and the smallest ones for d_f and J (Table 5). SPM and $\Delta\rho_f$ showed their lowest averaged values in early wet season, while D_{50} and w_s showed their lowest ones in wet season. d_f and J were maximum in the wet season.

5.3.1. SPM

The tidal variation of SPM (the highest at low tide, the lowest at high tide, with intermediate values slightly higher at ebb than flood) and its seasonal variation (the highest in the dry season, the lowest in the wet season) measured in the Cam-Nam Trieu estuary are consistent with the measurements by Piton et al. (2020b) in the nearby Van Uc estuary. Their regular sampling during 24 h-cycles in spring and neap tides at fixed stations, in dry and wet seasons, gives a refined analysis, and especially additional information on the spring-neap tide variability.

5.3.2. D_{50} and J

In this study, median aggregate sizes were calculated at 310 stations from in situ data of 15 transects. The depth-averaged D_{50} values over the whole size range of the LISST (1.48–212 μm) were higher in the dry season than in the wet or early wet season. This seasonal variation of D_{50} is consistent with the previous study in the Cam-Bach Dang estuary by Lefebvre et al. (2012), who showed that aggregates transfer from the coarser size classes (macroflocs, coarse microflocs) to finer ones in the wet season due to high turbulent energy (corresponding to low Kolmogorov microscales). The present results are in agreement with these previous ones, with a higher proportion of fine aggregates in the wet season than in the dry season (~35% vs. ~30%, respectively, at high tide) and a higher proportion of coarse aggregates in the dry season than in the wet season (33% vs. 27–28%, respectively, at high tide). Besides turbulence constraints, bigger aggregates in the dry season may also be linked to the abundance of transparent exopolymer particles (TEP), which promote sediment aggregation (van der Lee, 2000; Verney et al., 2009; Markussen and Andersen, 2013; Lee et al., 2017; Fettweis and Lee, 2017). The enhanced transfer from finer aggregates to coarser ones in the dry season is responsible for the reduction of J, the slope of the particle size distribution, at this period, already shown in this estuary (Mari et al., 2012).

In addition, the present study evidenced a consistent difference amongst surveys between averaged parameters in upper and lower parts of ETM, with higher D_{50} and lower J values in the lower ETM than in the upper ETM, in wet and dry seasons. Finally, if the maximum D_{50} in the lower ETM is observed at its center, it seems that it is observed in the upper ETM rather at its upstream and downstream boundaries, which reinforces the idea that distinct processes are responsible for their respective formation.

Piton et al. (2020b) give more detailed information in the tidal variability of D_{50} in the nearby Van Uc estuary. The maximum of SPM and D_{50} that was broadly observed in the present study was shown to be fully consistent with the Van Uc upper estuary in wet and dry seasons, but Piton et al. (2020b) also showed that the maximum of SPM and D_{50} did not occur at the same time in dry season (at higher salinity), D_{50} being then maximum at high tide or at ebb. The tidal variations of D_{50} may thus be different in upstream and downstream parts of the estuary.

5.3.3. Excess of density

During the three field surveys, the bulk excess of density of flocs varied in the range 44.8–595.1 kg m^{-3}. The average value of $\Delta\rho_f$ increased from early wet season (133.2 kg m^{-3}, during ebb stage, sampled at each season), to wet season (162.2 kg m^{-3}) and dry season (178.8 kg m^{-3}) (Tables 3, 5). These results are highly consistent with reported values of excess density in estuaries and coastal zones (Winterwerp, 2001; Fettweis, 2008; Guo et al., 2017). $\Delta\rho_f$ was seen to increase with increasing SPM (Fig. 8) and to decrease with increasing D_{50} (Fig. 9).

The slope of the $\Delta\rho_f$ - SPM relationship in log-log presentation is 0.30 in average, and varies from 0.12 at low tide to 0.82 at high tide. The increase of $\Delta\rho_f$ with increasing SPM has been observed by many authors, in natural environments like in laboratory experiments (Mhashhash et al., 2018). The slope seems to be lower in average in the Cam-Nam Trieu estuary than in other estuaries, most of them being located in temperate climate, with slopes between 0.61 (Humber) and 2.6 (Elbe) (van Leussen, 1994). However, we have to notice that, along a river like the Ems, van Leussen (2011) shown that the lowest slope was measured in the turbidity maximum.

A "theoretical" decrease of the bulk excess of density with D_{50} may be assessed from the fractal distribution of aggregates (eq. 6 and 7): since ρ_p varies little with the season (because ω varied few, between 0.85 and 0.92), the "theoretical" $\Delta\rho_f$ should vary proportionally to D^{d_f-3}, with d_f values around 2.0, i.e. almost proportionally to D^{-1}. In fact, the slope of the $\Delta\rho_f$ - D_{50} relationship in log-log, based on in situ measurements of excess of density and median diameter, is in average − 0.445 in this

study, close to the value (−0.42) found by Mikkelsen and Pejrup (2001) in coastal waters of Danemark using the same PSD device. This value is less than other slopes revealed in Cheseapeake Bay (−0.97; Gibbs, 1985) or in the Tamar estuary (between −0.76 and −1.92, Al Ani et al., 1991; −1.084, Fennessy et al., 1994; −0.99, Manning and Dyer, 1999), measured with other particle size meters and over different size ranges. From our measurements, the slope is very sensitive to the tidal stage, from the lowest value at low tide (−0.164) to the highest one at high tide (−1.199). Varying slopes during the tidal cycle were already reported in the literature, with higher slope at flood than at ebb (Schwartz et al., 2017). Although the average slope of the $\Delta\rho_f$ - D_{50} relationship derived from in situ measurements is not close to −1, we anyway checked a good qualitative agreement between its value and the variability of d_f, with higher slopes at high tide (when d_f is lower) that at low tide (Fig. 9b).

5.3.4. Fractal dimension

Smaller d_f values correspond to enhanced fragmentation and the formation of strenghter and smaller flocs (Kranenburg, 1994; Hill et al., 1998; Mikkelsen and Pejrup, 2000), with higher excess of density (Bowers et al., 2017). The seasonal variations of the flocs fractal dimension d_f in the Cam-Nam Trieu estuary, which is the highest in wet season, 2.0, and the lowest in dry season, 1.97, at ebb stage (Tables 2, 5) may be considered in parallel to the average volume concentration of fine aggregates during the transects which increased from the early wet season (23.9%) to the wet season (34.42%), and to the dry season (37.4%). The range of these values of d_f is consistent with earlier works (Winterwerp, 1998; Fettweis, 2008; Maggi, 2009; Verney et al., 2009; Guo et al., 2017) which showed that the flocs fractal dimension ranged from 1.4 to 2.7.

5.3.5. Settling velocity

The bulk settling velocity of aggregates calculated at 99 stations from measurements showed w_s varying in the range 0.03–0.55 mm s^{-1}, which is consistent with values obtained in other similar environments (Voulgaris and Meyers, 2004; Xia et al., 2004; Verney et al., 2009; Guo et al., 2017). Its seasonally averaged values over all transects, at high tide, varied from the lowest in wet season (0.11 mm s^{-1}, see Tables 4 and 5) to the highest in dry season (0.17 mm s^{-1}), with an intermediate value in early wet season (0.12 mm s^{-1}), in the same way than floc size. The literature showed that estuarine floc size depends at least on two main factors: turbulent mixing (e.g. Dyer, 1989; Eisma et al., 1997; Winterwerp, 1998; McAnally and Mehta, 2001; Fettweis et al., 2006; Manning and Schoellhamer, 2013), and the presence of TEPs (e.g. Logan et al., 1995; Passow et al., 2001; Mari et al., 2017). As it has been demonstrated by McCave (1984), Lefebvre et al. (2012) checked in this estuary that turbulence determine the maximum floc size at a given tidal stage. Mari et al. (2012) also showed that the sticking properties of TEPs in the Cam-Nam Trieu estuary suddenly increased from salinity 10 to 15 psu, stimulating an "aggregation web" (or a front of aggregation), likely related to microbial processes. Under the influence of TEPs, small mud flocs may aggregate into larger ones (Pejrup and Mikkelsen, 2010; Andersen and Pejrup, 2011). However, as already noticed about d_f variations and as seen on Fig. 12, w_s does not depend only on flocs size, and but also on other factors affecting aggregation, including: mineralogy (Winterwerp and van Kesteren, 2004); electrolytic levels which tend to be altered through salinity in an estuary (Krone, 1963), which can in turn affect the zeta-potential of clay particles (Chassagne et al., 2009); suspended sediment concentration (Burban et al., 1989; Winterwerp, 2006; Fettweis et al., 2014; Maerz et al., 2016); organic content (Kranck, 1984). In this study, although good correlations were obtained between w_s and SPM at some seasons, no global trend was observed.

In addition, the present study clearly evidenced a consistent difference between averaged parameters in upper and lower parts of ETM, with higher w_s values in the lower ETM than in the upper ETM, in wet and dry seasons.

5.4. On the processes governing the ETM patterns, its dynamics and the variability of the aggregate parameters

The material transported in rivers has a continuum in size from the soluble fraction (< 1 nm) to the particulate fraction (> 0.2 μm) via colloids (1 nm – 1 μm). The particulate fraction is itself made up of aggregates of mineral particles – rock fragments – and organic matter secreted by bacteria or resulting from the decomposition of plants, the organic matter serving as glue (Droppo, 2001). A distinction is generally made between microflocs (< 100 μm), strongly bound mineral particles glued together by organic matter, and macroflocs (> 100 μm), loose. In an estuary, the complex dynamics (gravity circulation, tidal asymmetry, seasonality of freshwater inputs) and the distribution of the associated salinity are constantly reflected in this matter, which therefore undergoes high variations on several time scales: interannual/climatic, seasonal, neap-spring tide cycle, tide cycle. An estuary is thus in constant dynamic equilibrium.

The change in size distribution (and settling velocity) of particles in the estuary as well as the increase in the particle load in the ETM can be explained by physical processes related to estuarine circulation or tidal pumping, physico-chemical processes linked to the colloid flocculation/deflocculation, bio-aggregation (the "aggregation web"), and their combination. Two major mechanisms are involved in sediment trapping at different locations of estuaries (Dyer, 1995; Burchard et al., 2018): in the salt wedge (and stratified waters) when estuarine circulation prevails, and upstream of the salinity front in the case of tidal pumping. The balance between these two main processes seems related to the magnitude of tidal range compared to the fresh water flow. For example, Allen et al. (1980) discussed the possibility that pure tidal processes (and especially tidal asymmetry) could trap sediment in the "freshwater" zone of the Gironde and the Aulne estuaries, and be dominant in low flow season, when the estuarine circulation is weaker.

Flocculation induced at very low salinities is another process that has been suggested for ETM formation (Postma, 1967; Gibbs et al., 1989). The turbidity that appears at very low salinities (from 0.1 psu to 1–3 psu) can be explained by the agglomeration of colloids, and Eisma (1986) detailed the importance of the reactivity of organic matter. Tidal pumping and chemical mechanisms probably coexist and add up to form the upstream part of the ETM and determine the characteristics of its aggregates.

Similarly, considering bio-aggregation at 10–15 psu associated with TEPs and microbial activities (Mari et al., 2012, 2017), gravitational circulation and biochemical mechanisms probably coexist and add to form the downstream part of the ETM and to determine its aggregate characteristics.

A double structure of ETM has already been observed in the Gironde estuary (Eisma, 1986; Gibbs et al., 1989) with a small turbidity peak at low salinity (less than 1 psu) and another one at around 3–8 psu (in May 1983), both with a local increase of microflocs and a decrease in fine aggregates (< 4 μm) (Eisma, 1986, his Fig. 5). Between these two peaks, at low salinity (~1–3 psu), Eisma observed a region of low turbidity and mainly fine aggregates with lower settling velocities, as also observed by Puels and Kuehl (1986) in the Elbe estuary. The first peak can be attributed to the salt flocculation: at low but increasing salinity (< 1 psu) the positively charged ions likely compensate for the repulsive force at the surface of the suspended particles that become attached. Migniot (1968) observed that the floc settling velocities gradually increase to reach their maximum value from ~2 psu. The decrease in settling velocity at ~1–3 psu may be attributed to a de-flocculation accompanied by a locally high concentration in carbohydrates (mucopolysaccharides or dissolved sugars mobilized from the microflocs), enhanced in winter, when biological activity is low (Eisma, 1986).

An additional remark can be made. Allen et al. (1980) mentioned that "the tidal trapping zone is generally further upstream than the density circulation node at the head of the salt intrusion". The upstream boundary of the ETM appears remarkably stable, all year round, at 0.1

psu (see Fig. 13a), and no transect showed the occurrence of any ETM in the freshwater. The explanation given by Allen et al. (1980) for the higher upwelling of particles in dry periods due to a greater influence of tidal processes is fully consistent with our observations. The present study shows that most of the particles are trapped in the downstream part during high flow periods when estuarine circulation is maximal, and that most of them are trapped in the upstream part during low flow periods, when estuarine circulation decreases and therefore the influence of tidal pumping is enhanced.

All these observations, reinforced by the literature, support the hypothesis that the two parts of the ETM can be attributed to two main mechanisms: the estuarine circulation for the downstream part, and the tidal effect for the upstream part. All year round, the amplitudes of the river flow and the spring tide combine in the Cam-Nam Trieu estuary without either process becoming negligible. Depending on the estuary, one process may be more dominant than the other. While tidal processes dominate in macrotidal estuaries (e.g. Mitchell, 2013) and estuarine circulation in microtidal estuaries (e.g. Kranck, 1981; Patchineelam and Kjerfve, 2004), mesotidal estuaries offer the possibility of a superposition of two mechanisms that create a local increase in turbidity at two distinct locations: an upstream maximum at very low salinities, and a downstream maximum in the salt wedge. The position of the ETM and the comparison of turbidity in its two parts on either side of the salt wedge can be a good indicator of the balance between the two main mechanisms responsible of its formation.

The effect of tidal pumping is indeed obvious when it brings particles upstream of the density circulation node, which may be the case in macrotidal estuaries. In mesotidal estuaries, it is possible to imagine that, when tidal pumping is limited and the tidal trapping zone is located downstream of the density circulation node, the resuspended marine particles transported towards the salt wedge by the tidal asymmetry are added to the particles settling in the river. A numerical model will allow in such a configuration to quantify the effect of the density circulation independently of the tide, the separate effects of each main tidal wave and its asymmetry on particle transport (e.g. Chernetsky et al., 2010), as well as their combination, in the formation of ETM.

Finally, the maximum D_{50} in the core of the lower ETM is consistent with the observation made by Kranck (1981) in the Miramichi microtidal estuary. To explain the coarsest bottom grain size we measured near the river mouth and the largest D_{50} systematically measured in the lower ETM, we can recall that the transport mechanism associated with estuarine circulation forms an efficient sorting (Postma, 1967; Schubel, 1968). Particles are transported seawards in the upper layer, fall and are carried landward in the salt wedge, with the coarser particles depositing in the middle to lower reaches of the estuary, downstream of the ETM.

6. Conclusion

The physico-chemical parameters along the mesotidal Cam-Nam Trieu estuary showed that an area of maximum turbidity developed around the salt wedge. The structure observed repeatedly on this estuary highlights the separation of two distinct zones of high turbidity separated by a zone of lower turbidity. The upstream part developed at very low salinity (from 0.1 psu) in well mixed waters, at Simpson parameter Φ between ~0.65 and 6–10; we called it the upper part of the ETM in this paper. A second maximum was observed in the salt wedge (i.e. in the lower layer of stratified waters), at Φ Simpson parameters >10 and salinity up to ~12–15 psu; we called it the downstream part of the ETM. Between these two parts, an area of locally decreasing turbidity was observed several times, and this area seemed to be longer in the wet season. Based on the literature, the downstream part is a result of gravitational circulation and the upstream part is associated with tidal asymmetry. These physical processes are most likely superimposed by chemical processes (colloid aggregation) in the upstream ETM and biochemical processes (TEPs-related) in the downstream ETM that modulate the parameters of the aggregates. The result is a double structure of the ETM, which may be observed in other estuaries, especially in mesotidal ones.

A seasonal variation of these ETMs and of their related parameters was inferred from the three surveys. In descending order, stronger ETMs occur in dry season than in early wet season and wet season. Their location changed seasonally, moving upstream in the dry season and downstream in the wet season. Only the upper ETM was observed in the riverine part of the estuary (until the river mouth) in wet season, the lower ETM, if any, moved off the river mouth in the bay. Turbidity was higher in the upper ETM in the dry season and higher in the lower ETM in the wet season. The flocs fractal dimensions had a small seasonal variation, with its highest values in wet season and its smallest ones in the dry season. Floc size, excess of density and settling velocity were the highest during dry season. All the observations analyzed in this paper were performed during spring tides. A complementary study on the nearby Van Uc estuary gives additional information on the variability during the daily tidal cycle at high frequency and during the lunar tidal cycle (neap-spring tides) (Piton et al., 2020b).

A consequence of this double structure of ETM in the Cam-Nam Trieu estuary is that we should be aware of it when observing the turbidity structures using remote sensing: only the upper part of the ETM, which develops until the surface, will be observable from satellite imagery. The lower part of the ETM, below the turbid surface layer of several meter deep, cannot be observed by passive sensors (see, e.g., Ouillon, 2003).

The analysis of phenomena observed in estuaries is all the more complex as the scientific communities of physicists, specialists in particle dynamics, chemists and microbiologists have approaches, tools and even study variables that differ and complement each other (Ouillon, 2018). In order to make progress in the development of broader concepts encompassing physics, chemistry and microbiology, the skills of these disciplines must be encouraged to come together in joint campaigns and intensify their exchanges so that we can be more precise about the key processes along the estuary at different periods. For example, it would be particularly relevant to better know the quantity of particulate matter created in the estuary by the aggregation of colloids, and under what conditions (salinity, turbulence, abundance of organic matter, etc.). It is possible to make progress in the understanding of physico-chemical processes using numerical models, in predictor-corrector mode or using data assimilation techniques, but it is felt that a model will never be sufficient to represent everything, in a tropical mesotidal estuary such as the Cam-Nam Trieu, if it does not also integrate the microbial loop and the polymers, including dissolved sugars.

Declaration of Competing Interest

The authors declare that they have no known competing financial interests or personal relationships that could have appeared to influence the work reported in this paper.

Acknowledgements

This work was financed by the Science and Technological Cooperation Program between the Vietnam Academy of Sciences and Technology (VAST) and the French Research Institute for Development (IRD), QTFR01.01/20-21. This paper is also a contribution to the LOTUS International Joint Laboratory (lotus.usth.edu.vn) and benefited from the support of VAST05.05/21-22 and NĐT.97.BE/20 projects. The authors warmly thank the editor and the two anonymous reviewers for their suggestions to improve the article.

Appendix 1

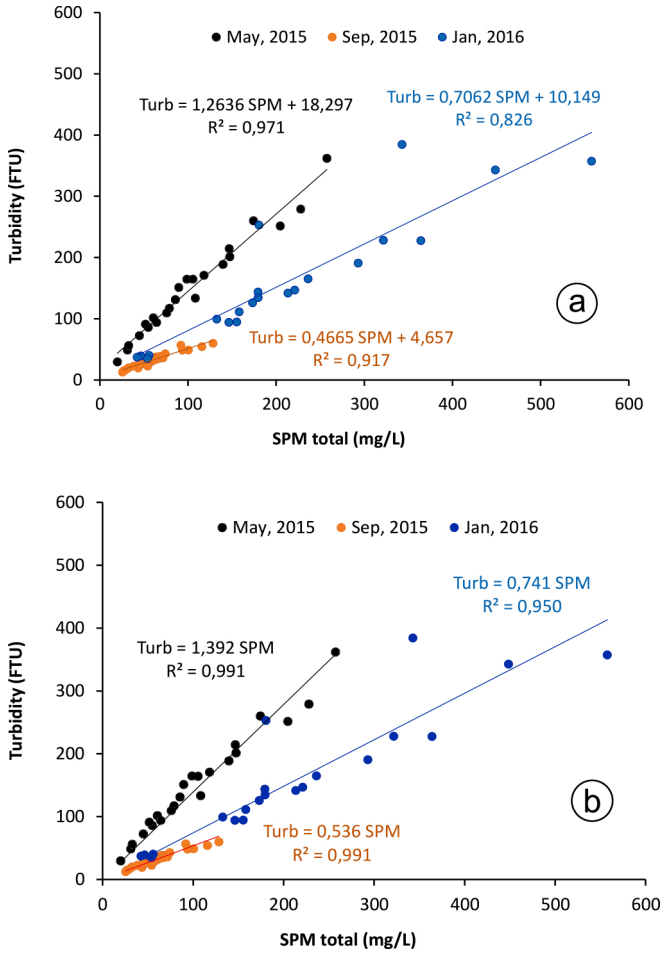

Fig. A1. Best correlated linear relationships between Turbidity (in FTU) and SPM concentrations (in mg L^{-1}) during the three surveys: (A) without passing through the y-intercept, (B) passing through the y-intercept.

References

Abascal-Zorrilla, N., Vantrepotte, V., Huybrechts, N., Ngoc, D.D., Anthony, E.J., Gardel, A., 2020. Dynamics of the estuarine turbidity maximum zone from Landsat-8 data: the case of the Maroni River Estuary, French Guiana. Remote Sens. 12, 2173. https://doi.org/10.3390/rs12132173.

Achite, M., Ouillon, S., 2007. Suspended sediment transport in a semiarid watershed, Wadi Abd, Algeria (1973-1995). J. Hydrol. 343 (3–4), 187–202. https://doi.org/10.1016/j.jhydrol.2007.06.026.

Agrawal, Y.C., Pottsmith, H.C., 2000. Instruments for particle size and settling velocity observations in sediment transport. Mar. Geol. 168, 89–114. https://doi.org/10.1016/S0025-3227(00)00044-X.

Al Ani, S., Dyer, K.R., Huntley, D.A., 1991. Measurement of the influence of salinity on floc density and strength. Geo-Mar. Lett. 11 (3–4), 154–158. https://doi.org/10.1007/BF02431002.

Allen, G.P., Castaing, P., 1973. Suspended sediment transport from the Gironde estuary (France) onto the adjacent continental shelf. Mar. Geol. 14, 47–53. https://doi.org/10.1016/0025-3227(73)90011-X.

Allen, G.P., Salomon, J.C., Bassoullet, P., du Penhoat, Y., de Grandpré, C., 1980. Effects of tides on mixing and suspended sediment transport in macrotidal estuaries. Sediment. Geol. 26, 69–90. https://doi.org/10.1016/0037-0738(80)90006-8.

Andersen, T.J., Pejrup, M., 2011. Biological influences on sediment behavior and transport. In: Treatise on Estuarine and Coastal Science. Elsevier Inc. https://doi.org/10.1016/B978-0-12-374711-2.00217-5.

Andrews, S., Nover, D., Schladow, S., 2010. Using laser diffraction data to obtain accurate particle size distributions: the role of particle composition. Limnol. Oceanogr. Methods 8, 507–526. https://doi.org/10.4319/lom.2010.8.507.

Babin, M., Morel, A., Fournier-Sicre, V., Fell, F., Stramski, D., 2003. Light scattering properties of marine particles in coastal and open ocean waters as related to the particle mass concentration. Limnol. Oceanogr. 843–859. https://doi.org/10.4319/lo.2003.48.2.0843.

Bader, H., 1970. The hyperbolic distribution of particle sizes. J. Geophys. Res. 75, 2822–2830. https://doi.org/10.1029/JC075i015p02822.

Boss, E., Twardowski, M.S., Herring, S., 2001. Shape of the particulate beam attenuation spectrum and its inversion to obtain the shape of the particulate size distribution. Appl. Opt. 40, 4885–4893. https://doi.org/10.1364/AO.40.004885.

Bowden, K.F., 1984. Turbulence and mixing in estuaries. In: Kennedy, V.S. (Ed.), The Estuary as a Filter. Academic Press, Orlando, FL, USA, pp. 15–26. https://doi.org/10.1016/B978-0-12-405070-9.50008-6.

Bowers, D.G., McKee, D., Jago, C.F., Nimmo-Smith, W.A.M., 2017. The area-to-mass ratio and fractal dimension of marine flocs. Estuar. Coast. Shelf Sci. 189, 224–234. https://doi.org/10.1016/j.ecss.2017.03.026.

Brenon, I., Le Hir, P., 1999. Modelling the turbidity maximum in the Seine estuary (France): identification of formation processes. Estuar. Coast. Shelf Sci. 49, 525–544. https://doi.org/10.1006/ecss.1999.0514.

Burban, P.-Y., Lick, W., Lick, J., 1989. The flocculation of fine-grained sediments in estuarine waters. J. Geophys. Res. 94 (C6), 8323–8330. https://doi.org/10.1029/JC094iC06p08323.

Burchard, H., Schuttelaars, H.M., Ralston, D.K., 2018. Sediment trapping in estuaries. Annu. Rev. Mar. Sci. 10, 371–395. https://doi.org/10.1146/annurev-marine-010816-060535.

Capo, S., Sottolochio, A., Brenon, I., Castaing, P., Ferry, L., 2006. Morphology, hydrography and sediment dynamics in a mangrove estuary: the Konkoure Estuary, Guinea. Mar. Geol. 230 (3–4), 199–215. https://doi.org/10.1016/j.margeo.2006.05.003.

Chassagne, C., Mietta, F., Winterwerp, J.C., 2009. Electrokinetic study on kaolinite suspensions. J. Colloid Interface Sci. 336 (1), 352–359. https://doi.org/10.1016/j.jcis.2009.02.052.

Chernetsky, A.S., Schuttelaars, H.M., Talke, S.A., 2010. The effect of tidal asymmetry and temporal settling lag on sediment trapping in tidal estuaries. Ocean Dyn. 60, 1219–1241. https://doi.org/10.1007/s10236-010-0329-8.

Coleman, J.M., Wright, L.D., 1978. Sedimentation in an arid macrotidal alluvial river system: Ord River, Western Australia. J. Geol. 86, 621–642. https://doi.org/10.1086/649728.
Droppo, I., 2001. Rethinking what constitutes suspended sediment. Hydrol. Process. 15, 1551–1564. https://doi.org/10.1002/hyp.228.
Duy Vinh, V., Ouillon, S., Van Uu, D., 2018. Estuarine turbidity maxima and variations of aggregate parameters in the Cam-Nam Trieu Estuary, North Vietnam, in Early Wet Season. Water 10, 68. https://doi.org/10.3390/w10010068.
Dyer, K.R., 1989. Sediment processes in estuaries: future research requirements. J. Geophys. Res. 94 (C10), 14,327–14,339. https://doi.org/10.1029/JC094iC10p14327.
Dyer, K.R., 1995. Chapter 14 Sediment processes in estuaries. In: Perillo, G.M.E. (Ed.), Development in Sedimentology, 53, pp. 423–449. https://doi.org/10.1016/S0070-4571(05)80034-2.
Eisma, D., 1986. Flocculation and de-flocculation of suspended matter in estuaries. Neth. J. Sea Res. 20 (2/3), 183–199. https://doi.org/10.1016/0077-7579(86)90041-4.
Eisma, D., Dyer, K.R., van Leussen, W., 1997. The in-situ determination of the settling velocities of suspended fine-grained sediment — a review. In: Burt, N., Parker, R., Watts, J. (Eds.), Cohesive Sediments — Proc. of INTERCOH Conf. (Wallingford, England). John Wiley & Son, Chichester, pp. 17–44.
Fennessy, M.J., Dyer, K.R., Huntley, D.A., 1994. INSSEV — an instrument to measure the size and settling velocity of flocs in situ. Mar. Geol. 117 (1–4), 107–117. https://doi.org/10.1016/0025-3227(94)90009-4.
Festa, J.F., Hansen, D.V., 1978. Turbidity maxima in partially mixed estuaries: a two-dimensional numerical model. Est. Coast. Shelf Sci. 7 (4), 347–360. https://doi.org/10.1016/0302-3524(78)90087-7.
Fettweis, M., 2008. Uncertainty of excess density and settling velocity of mud flocs derived from in situ measurements. Estuar. Coast. Shelf Sci. 78, 426–436. https://doi.org/10.1016/j.ecss.2008.01.007.
Fettweis, M., Baeye, 2015. M. Seasonal variation in concentration, size and settling velocity of muddy marine flocs in the benthic boundary layer. J. Geophys. Res. Oceans 120, 5648–5667. https://doi.org/10.1002/2014JC010644.
Fettweis, M., Lee, B.J., 2017. Spatial and seasonal variation of biomineral suspended particulate matter properties in high-turbid nearshore and low-turbid offshore zones. Water 9, 694. https://doi.org/10.3390/w9090694.
Fettweis, M., Sas, M., Monbaliu, J., 1998. Seasonal, Neap-spring and tidal variation of cohesive sediment concentration in the Scheldt estuary, Belgium. Estuar. Coast. Shelf Sci. 47, 21–36. https://doi.org/10.1006/ecss.1998.0338.
Fettweis, M., Francken, F., Pison, V., Van den Eynde, D., 2006. Suspended particulate matter dynamics and aggregate sizes in a high turbidity area. Mar. Geol. 235, 63–74. https://doi.org/10.1016/j.margeo.2006.10.005.
Fettweis, M., Baeye, M., Van der Zande, D., Van den Eynde, D., Lee, B.J., 2014. Seasonality of floc strength in the southern North Sea. J. Geophys. Res. Oceans 119, 1911–1926. https://doi.org/10.1002/2013JC009750.
Geyer, W.R., Woodruff, J.D., Traykovski, P., 2001. Sediment transport and trapping in the Hudson River Estuary. Estuaries 24, 670–679. https://doi.org/10.2307/1352875.
Gibbs, R.J., 1985. Estuarine flocs — their size, settling velocity and density. J. Geophys. Res. 90 (NC2), 3249–3251. https://doi.org/10.1029/JC090iC02p03249.
Gibbs, R.J., Tshudy, D.M., Konwar, L., Martin, J.M., 1989. Coagulation and transport of sediments in the Gironde Estuary. Sedimentology 36, 987–999. https://doi.org/10.1111/j.1365-3091.1989.tb01536.x.
Graham, G.W., Davies, E.J., Nimmo-Smith, W.A.M., Bowers, D.G., Braithwaite, K.M., 2012. Interpreting LISST-100X measurements of particles with complex shape using digital in-line holography. J. Geophys. Res. 117, C05034 https://doi.org/10.1029/2011JC007613.
Guo, C., He, Q., Guo, L., Winterwerp, J.C., 2017. A study of in-situ sediment flocculation in the turbidity maxima of the Yangtze Estuary. Estuar. Coast. Shelf Sci. 191, 1–9. https://doi.org/10.1016/j.ecss.2017.04.001.
Hill, P.S., Syvitski, J.P., Cowan, E.A., Powell, R.D., 1998. In situ observations of floc settling velocities in Glacier Bay, Alaska. Mar. Geol. 145, 85–94. https://doi.org/10.1016/S0025-3227(97)00109-6.
Jackson, G., Maffione, D., Costello, A., Alldredge, B., Logan, B., Dam, H., 1997. Particle size spectra between 1 μm and 1 cm at Monterey Bay determined using multiple instruments. Deep Sea Res. I 44, 1739–1767. https://doi.org/10.1016/S0967-0637(97)00029-0.
Jalón-Rojas, I., Schmidt, S., Sottolichio, A., 2015. Turbidity in the fluvial Gironde Estuary (southwest France) based on 10-year continuous monitoring: sensitivity to hydrological conditions. Hydrol. Earth Syst. Sci. 19, 2805–2819. https://doi.org/10.5194/hess-19-2805-2015.
Jay, D.A., Musiak, J.D., 1994. Particle trapping in estuarine tidal flows. J. Geophys. Res. 99, 20445–20461. https://doi.org/10.1029/94JC00971.
Jouon, A., Ouillon, S., Douillet, P., Lefebvre, J.-P., Fernandez, J.-M., Mari, X., Froidefond, J.-M., 2008. Spatio-temporal variability in suspended particulate matter concentration and the role of aggregation on size distribution in a coral reef lagoon. Mar. Geol. 256, 36–48. https://doi.org/10.1016/j.margeo.2008.09.008.
Kirby, R., Parker, W.R., 1983. Distribution and behavior of fine sediment in the Severn Estuary and Inner Bristol Channel, UK. Can. J. Fish. Aquat. Sci. 40, 83–95. https://doi.org/10.1139/f83-271.
Kistner, D.A., Pettigrew, N.R., 2001. A variable turbidity maximum in the Kennebec Estuary. Estuaries 24, 680–687. https://doi.org/10.2307/1352876.
Kranck, K., 1981. Particulate matter grain-size characteristics and flocculation in a partially-mixed estuary. Sedimentology 28 (1), 107–114. https://doi.org/10.1111/j.1365-3091.1981.tb01667.x.
Kranck, K., 1984. The role of flocculation in the filtering of particulate matter in estuaries. In: Kennedy, V. (Ed.), The Estuary as a Filter. Academic Press, Orlando, FL, USA, pp. 159–175. https://doi.org/10.1016/B978-0-12-405070-9.50014-1.
Kranenburg, C., 1994. The fractal structure of cohesive sediment aggregates. Estuar. Coast. Shelf Sci. 39, 451–460. https://doi.org/10.1016/S0272-7714(06)80002-8.
Krone, R.B., 1963. A Study of Rheological Properties of Estuarial Sediments. Report No. 63–68. Hyd. Eng. Lab. and Sanitary Eng. Lab., University of California, Berkeley.
Lee, B.J., Hur, J., Toorman, E.A., 2017. Seasonal variation in flocculation potential of river water: roles of the organic matter pool. Water 9, 335. https://doi.org/10.3390/w9050335.
Lefebvre, J.P., Ouillon, S., Vinh, V.D., Arfi, R., Panche, J.Y., Mari, X., Van Thuoc, C., Torréton, J.P., 2012. Seasonal variability of cohesive sediment aggregation in the Bach Dang-Cam Estuary, Haiphong (Vietnam). Geo-Mar. Lett. 32, 103–121. https://doi.org/10.1007/s00367-011-0273-8.
Logan, B.E., Passow, U., Alldredge, A.L., Grossart, H.-P., Simon, M., 1995. Rapid formation and sedimentation of large aggregates is predictable from coagulation rates (half-lives) of transparent exopolymer particles (TEP). Deep-Sea Res. 42 (1), 203–214. https://doi.org/10.1016/0967-0645(95)00012-F.
Maerz, J., Hofmeister, R., van der Lee, E.M., Gräwe, U., Riethmüller, R., Wirtz, K.W., 2016. Maximum sinking velocities of suspended particulate matter in a coastal transition zone. Biogeosciences 13, 4863–4876. https://doi.org/10.5194/bg-13-4863-2016.
Maggi, F., 2009. Biological flocculation of suspended particles in nutrient-rich aqueous ecosystems. J. Hydrol. 376, 116–125. https://doi.org/10.1016/j.jhydrol.2009.07.040.
Manning, A.J., Dyer, K.R., 1999. A laboratory examination of floc characteristics with regard to turbulent shearing. Mar. Geol. 160 (1–2), 147–170. https://doi.org/10.1016/S0025-3227(99)00013-4.
Manning, A.J., Schoellhamer, D.H., 2013. Factors controlling floc settling velocity along a longitudinal estuarine transect. Mar. Geol. 345, 266–280. https://doi.org/10.1016/j.margeo.2013.06.018.
Many, G., Bourrin, F., Durrieu de Madron, X., Pairaud, I., Gangloff, A., Doxaran, D., Ody, A., Verney, R., Menniti, C., Le Berre, D., et al., 2016. Particle assemblage characterization in the Rhone river ROFI. J. Mar. Syst. 157, 39–51. https://doi.org/10.1016/j.jmarsys.2015.12.010.
Mari, X., Torréton, J.P., Chu, V.T., Lefebvre, J.P., Ouillon, S., 2012. Aggregation dynamics along a salinity gradient in the Bach Dang estuary, North Vietnam. Estuar. Coast. Shelf Sci. 96, 151–158. https://doi.org/10.1016/j.ecss.2011.10.028.
Mari, X., Passow, U., Migon, C., Burd, A.B., Legendre, L., 2017. Transparent exopolymer particles: effects on carbon cycling in the ocean. Prog. Oceanogr. 151, 13–37. https://doi.org/10.1016/j.pocean.2016.11.002.
Markussen, T.N., Andersen, T.J., 2013. A simple method for calculating in situ floc settling velocities based on effective density functions. Mar. Geol. 344, 10–18. https://doi.org/10.1016/j.margeo.2013.07.002.
McAnally, W.H., Mehta, A.J., Mehta, A.J., 2001. Collisional aggregation of fine estuarine sediments. In: McAnally, W.H. (Ed.), Coastal and Estuarine Fine Sediment Processes — Proc. in Mar. Sci, vol. 3. Elsevier, Amsterdam, pp. 19–39. https://doi.org/10.1016/S1568-2692(00)80110-2.
McCave, I.N., 1984. Size spectra and aggregation of suspended particles in the deep ocean. Deep-Sea Res. 31, 329–352. https://doi.org/10.1016/0198-0149(84)90088-8.
Meybeck, M., Laroche, L., Dürr, H.H., Syvitski, J.P.M., 2003. Global variability of daily total suspended solids and their fluxes in rivers. Glob. Planet. Change 39, 65–93. https://doi.org/10.1016/S0921-8181(03)00018-3.
Mhashhash, A., Bockelmann-Evans, B., Pan, S.J., 2018. Effect of hydrodynamics factors on sediment flocculation processes in estuaries. J. Soils Sediments 18, 3094–3103. https://doi.org/10.1007/s11368-017-1837-7.
Migniot, C., 1968. Etude des propriétés physiques de différents sédiments très fins et de leur comportement sous des actions hydrodynamiques. La Houille Blanche 7, 591–620. https://doi.org/10.1051/lhb/1968041.
Mikkelsen, O.A., Pejrup, M., 2000. In situ particle size spectra and density of particle aggregates in a dredging plume. Mar. Geol. 170, 443–459. https://doi.org/10.1016/S0025-3227(00)00105-5.
Mikkelsen, O.A., Pejrup, M., 2001. The use of a LISST-100 laser particle sizer for in-situ estimates of floc size, density and settling velocity. Geo-Mar. Lett. 20 (4), 187–195. https://doi.org/10.1007/s003670100064.
Mikkelsen, O.A., Hill, P.S., Milligan, T.G., Chant, R.J., 2005. In situ particle size distributions and volume concentrations from a LISST-100 laser particle sizer and a digital floc camera. Cont. Shelf Res. 25, 1959–1978. https://doi.org/10.1016/j.csr.2005.07.001.
Miles, J., 1986. Richardson's criterion for the stability of stratified shear flow. Phys. Fluids 29, 3470. https://doi.org/10.1063/1.865812.
Minh, N.N., Marchesiello, P., Lyard, F., Ouillon, S., Cambon, G., Allain, D., Van Uu, D., 2014. Tidal characteristics of the Gulf of Tonkin. Cont. Shelf Res. 91, 37–56. https://doi.org/10.1016/j.csr.2014.08.003.
Mitchell, S.B., 2013. Turbidity maxima in four macrotidal estuaries. Ocean Coast. Manag. 79, 62–69. https://doi.org/10.1016/j.ocecoaman.2012.05.030.
Mitchell, S.B., Uncles, R.J., 2013. Estuarine sediments in macrotidal estuaries: future research requirements and management challenges. Ocean Coast. Manag. 79, 97–100. https://doi.org/10.1016/j.ocecoaman.2012.05.007.
Officer, C.B., 1981. Physical dynamics of estuarine suspended sediments. Mar. Geol. 40, 1–14. https://doi.org/10.1016/0025-3227(81)90039-6.
Olsen, C.R., Simpson, H.J., Bopp, R.F., Williams, S.C., Peng, T.H., Deck, B.L., 1978. A geochemical analysis of the sediments and sedimentation in the Hudson estuary. J. Sediment. Petrol. 48, 401–418. https://doi.org/10.1306/212F7496-2B24-11D7-8648000102C1865D.

Orseau, S., Lesourd, S., Huybrechts, N., Gardel, A., 2017. Hydro-sedimentary processes of a shallow tropical estuary under Amazon influence. The Mahury Estuary, French Guiana. Est. Coast. Shelf Sci. 189, 252–266. https://doi.org/10.1016/j.ecss.2017.01.011.

Ouillon, S., 2003. An inversion method for reflectance in stratified turbid waters. Int. J. Remote Sens. 24 (3), 535–548. https://doi.org/10.1080/01431160304986.

Ouillon, S., 2018. Why and how do we study sediment transport? Focus on coastal zones and ongoing methods. Water 10, 390. https://doi.org/10.3390/w10040390.

Passow, U., Shipe, R.F., Murray, A., Pak, D.K., Brzezinski, M.A., Alldredge, A.L., 2001. The origin of transparent exopolymer particles (TEP) and their role in the sedimentation of particulate matter. Cont. Shelf Res. 21, 327–346. https://doi.org/10.1016/S0278-4343(00)00101-1.

Patchineelam, S.M., Kjerfve, B., 2004. Suspended sediment variability on seasonal and tidal time scales in the Winyah Bay estuary, South Carolina, USA. Est. Coast. Shelf Sci. 59, 307–318. https://doi.org/10.1016/j.ecss.2003.09.011.

Pejrup, M., Mikkelsen, O.A., 2010. Factors controlling the field settling velocity of cohesive sediment in estuaries. Est. Coast. Shelf Sci. 87 (2), 177–185. https://doi.org/10.1016/j.ecss.2009.09.028.

Pinet, S., Martinez, J.M., Ouillon, S., Lartiges, B., Villar, R.E., 2017. Variability of apparent and inherent optical properties of sediment-laden waters in large river basins – lessons from in situ measurements and bio-optical modeling. Opt. Express 25, A283–A310. https://doi.org/10.1364/OE.25.00A283.

Piton, V., Herrmann, M., Lyard, F., Marsaleix, P., Duhaut, T., Allain, D., Ouillon, S., 2020a. Sensitivity study on the main tidal constituents of the Gulf of Tonkin by using the frequency-domain tidal solver in T-UGOm. Geosci. Model Dev. 13, 1583–1607. https://doi.org/10.5194/gmd-13-1583-2020.

Piton, V., Ouillon, S., Vinh, V.D., Many, G., Herrmann, M., Marsaleix, P., 2020b. Seasonal and tidal variability of the hydrology and suspended particulate matter in the Van Uc estuary, Red River, Vietnam. J. Mar. Syst. 211, 103403. https://doi.org/10.1016/j.jmarsys.2020.103403.

Postma, H., 1967. Sediment transport and sedimentation in the estuarine environment. In: Lauff, G.H. (Ed.), Estuaries. American Association Advanced Scientific Publication, Washington, DC, USA, pp. 158–179.

Puels, W., Kuehl, H., 1986. Field measurements of the settling velocities of estuarine flocs. In: Proceedings of the 3rd International Symposium on River Sedimentation, 31. The University of Mississippi, Jackson, pp. 525–536.

Rao, V.P., Shynu, R., Kessarkar, P.M., Sundar, D., Michael, G.S., Narvekar, T., Blossom, V., Mehar, P., 2011. Suspended sediment dynamics on a seasonal scale in the Mandovi and Zuari estuaries, central west coast of India. Est. Coast. Shelf Sci. 91, 78–86. https://doi.org/10.1016/j.ecss.2010.10.007.

Sanford, L.P., Suttles, S.E., Halka, J.P., 2001. Reconsidering the physics of the Chesapeake Bay estuarine turbidity maximum. Estuaries 24, 655–669. https://doi.org/10.2307/1352874.

Sanford, L.P., Dickhudt, P.J., Rubiano-Gomez, L., Yates, M., Suttles, S.E., Friedrichs, C.T., Fugate, D.D., Romine, H., 2005. Variability of suspended particle concentrations, sizes, and settling velocities in the Chesapeake Bay turbidity maximum. In: Droppo, I.G., Leppard, G.G., Liss, S.N., Milligan, T.G. (Eds.), Flocculation in Natural and Engineered Environmental Systems. CRC Press, Boca Raton, FL, USA, pp. 211–236.

Schoellhamer, D.H., 2001. Influence of salinity, bottom topography, and tides on locations of estuarine turbidity maxima in northern San Francisco Bay. In: McAnally, W.H., Mehta, A.J. (Eds.), Coastal and Estuarine Fine Sediment Transport Processes. Elsevier Science B.V, pp. 343–357.

Schubel, J.R., 1968. Turbidity maximum of the northern Chesapeake Bay. Science 161, 1013–1015. https://doi.org/10.1126/science.161.3845.1013.

Schwartz, C., Cox, T., van Engeland, T., van Oevelen, D., van Belzen, J., van de Koppel, J., Soetaert, K., Bouma, T.J., Meire, P., Temmerman, S., 2017. Field estimates of floc dynamics and settling velocities in a tidal creek with significant along-channel gradients in velocity and SPM. Est. Coast. Shelf Sci. 197, 221–235. https://doi.org/10.1016/j.ecss.2017.08.041.

Simpson, J.H., Allen, C.M., Morris, N.C.G., 1978. Fronts on the continental shelf. J. Geophys. Res. 83, 4607–4614. https://doi.org/10.1029/JC083iC09p04607.

Sottolichio, A., Castaing, P., 1999. A synthesis on seasonal dynamics of highly concentrated structures in the Gironde estuary. Comp. Rend. Acad. Sci. Paris IIa 329, 895–900. https://doi.org/10.1016/S1251-8050(00)88634-6.

Sottolichio, A., Le Hir, P., Castaing, P., 2000. Modeling mechanisms for the stability of the turbidity maximum in the Gironde estuary, France. Proc. Mar. Sci. 3, 373–386. https://doi.org/10.1016/S1568-2692(00)80132-1.

Stokes, G.G., 1851. On the effect of the internal friction of fluids on the motion of pendulums. In: Transaction Cambridge Philosophical Society (Printed at the Pitt Press: Cambridge, UK, Vol. IX, pp. 8–106. Reprinted In Mathematical and Physical Papers, 2nd ed., Johnson Reprint Corp: New York, NY, USA, 1966, Volume 3).

Toublanc, F., Brenon, I., Coulombier, T., 2016. Formation and structure of the turbidity maximum in the macrotidal Charente estuary (France): influence of fluvial and tidal forcing. Estuar. Coast. Shelf Sci. 169, 1–14. https://doi.org/10.1016/j.ecss.2015.11.019.

Traykovski, P., Latter, R., Irish, J.D., 1999. A laboratory evaluation of the laser in situ scattering and transmissometery instrument using natural sediments. Mar. Geol. 159, 355–367. https://doi.org/10.1016/S0025-3227(98)00196-0.

Traykovski, P., Geyer, W.R., Sommerfield, C., 2004. Rapid sediment deposition and fine-scale strata formation in the Hudson estuary. J. Geophys. Res. 109, F02004 https://doi.org/10.1029/2003JF000096.

Uncles, R.J., Stephens, J.A., 1993. Nature of the turbidity maximum in the Tamar Estuary, UK. Estuar. Coast. Shelf Sci. 36, 413–431. https://doi.org/10.1006/ecss.1993.1025.

Uncles, R.J., Easton, A.E., Griffiths, M.L., Harris, C., Howland, R.J.M., King, R.S., Morris, A.W., Plummer, D.H., 1999. Seasonality of the turbidity maximum in the Humber-Ouse Estuary, UK. Mar. Pollut. Bull. 37 (3–7), 206–215. https://doi.org/10.1016/S0025-326X(98)90157-6.

Uncles, R.J., Stephens, J.A., Smith, R.E., 2002. The dependence of estuarine turbidity on tidal intrusion length, tidal range and residence time. Cont. Shelf Res. 22, 1835–1856. https://doi.org/10.1016/S0278-4343(02)00041-9.

Uncles, R.J., Stephens, J.A., Harris, C., 2006. Runoff and tidal influences on the estuarine turbidity maximum of a highly turbid system: the upper Humber and Ouse Estuary, UK. Mar. Geol. 235, 213–228. https://doi.org/10.1016/j.margeo.2006.10.015.

van der Lee, W.T.B., 2000. Temporal variation of floc size and settling velocity in the Dollard estuary. Cont. Shelf Res. 20 (12−13), 1495–1511. https://doi.org/10.1016/S0278-4343(00)00034-0.

van der Lee, E.M., Bowers, D., Kyte, E., 2009. Remote sensing of temporal and spatial patterns of suspended particle size in the Irish Sea in relation to the Kolmogorov microscale. Cont. Shelf Res. 29, 1213–1225. https://doi.org/10.1016/j.csr.2009.01.016.

van Leussen, W., 1994. Estuarine Macroflocs and Their Role in Fine-grained Sediment Transport. PhD Thesis. University of Utrecht.

van Leussen, W., 2011. Macroflocs, fine-grained sediment transports, and their longitudinal variations in the Ems estuary. Ocean Dyn. 61, 387–401. https://doi.org/10.1007/s10236-011-0384-9.

Verney, R., Lafite, R., Brun Cottan, J.C., 2009. Flocculation potential of natural estuarine particles: the importance of environmental factors and of the spatial and seasonal variability of suspended particulate matter. Estuar. Coast. 32, 678–693. https://doi.org/10.1007/s12237-009-9160-1.

Vinh, V.D., Uu, D.V., 2013. The influence of wind and oceanographic factors on characteristics of suspended sediment transport in Bach Dang estuary. J. Mar. Sci. Technol. 3, 216–226. https://doi.org/10.15625/1859-3097/13/3/3526.

Vinh, V.D., Ouillon, S., Thanh, T.D., Chu, L.V., 2014. Impact of the Hoa Binh dam (Vietnam) on water and sediment budgets in the Red River basin and delta. Hydrol. Earth Syst. Sci. 18, 3987–4005. https://doi.org/10.5194/hess-18-3987-2014.

Voulgaris, G., Meyers, S.T., 2004. Temporal variability of hydrodynamics, sediment concentration and sediment settling velocity in a tidal creek. Cont. Shelf Res. 24, 1659–1683. https://doi.org/10.1016/j.csr.2004.05.006.

Winterwerp, J.C., 1998. A simple model for turbulence induced flocculation of cohesive sediment. J. Hydraul. Res. 36, 309–326. https://doi.org/10.1080/00221689809498621.

Winterwerp, J.C., 2001. Stratification effects by cohesive and noncohesive sediment. J. Geophys. Res. 106, 22559–22574. https://doi.org/10.1029/2000JC000435.

Winterwerp, J.C., 2006. A heuristic formula for turbulence-induced flocculation of cohesive sediment. Estuar. Coast. Shelf Sci. 68, 195–207. https://doi.org/10.1016/j.ecss.2006.02.003.

Winterwerp, J.C., van Kesteren, W.G.M., 2004. Introduction to the physics of cohesive sediment in the marine environment. In: van Loon, T. (Ed.), Developments in Sedimentology, 56. Elsevier, Amsterdam (466 pp.).

Wolanski, E., Ngoc Huan, N., Trong Dao, L., Huu Nhan, N., Ngoc Thuy, N., 1996. Fine-sediment dynamics in the Mekong River estuary, Vietnam. Est. Coast. Shelf Sci. 43, 565–582. https://doi.org/10.1006/ecss.1996.0088.

Xia, X.M., Li, Y., Yang, H., Wu, C.Y., Sing, T.H., Pong, H.K., 2004. Observations on the size and settling velocity distributions of suspended sediment in the Pearl River Estuary, China. Cont. Shelf Res. 24, 1809–1826. https://doi.org/10.1016/j.csr.2004.06.009.